Functional and structural insights into the interaction and multi-step activation of bacterial ExoY nucleotidyl cyclases toxins by profilin-bound G-actin

Magda Teixeira-Nunes[1], Pascal Retailleau[2], Dorothée Raoux-Barbot[3], Martine Comisso[1], Anani Amegan Missinou[1], Christophe Velours[1,#], Stéphane Plancqueel[1], Daniel Ladant[3], Undine Mechold[3], Louis Renault[1*]

[1] Université Paris-Saclay, CEA, CNRS, Institute for Integrative Biology of the Cell (I2BC), 91198, Gif-sur-Yvette, France

[2] ICSN, CNRS, Université Paris Saclay, 1 avenue de la terrasse, 91190, Gif-sur-Yvette, France.

[3] Institut Pasteur, Université Paris Cité, CNRS URA3528, Unité de Biochimie des Interactions macromoléculaires, Département de Biologie Structurale et Chimie, 25-28 rue du Docteur Roux, 75724 Paris cedex 15, France

[#] present address: Fundamental Microbiology and Pathogenicity Laboratory, UMR 5234 CNRS-University of Bordeaux, SFR TransBioMed, 33076 Bordeaux, France

[*]Correspondence: louis.renault@i2bc.paris-saclay.fr

Abstract

ExoY virulence factors belong to a family of invasive bacterial nucleotidyl cyclase (NC) toxins that are activated by specific eukaryotic cofactors and overproduce purine and pyrimidine cyclic nucleotides inside eukaryotic host cells. The molecular and mechanistic details underlying their activation and catalytic specificities are only partially understood. ExoY NC toxins use monomeric (G-actin) or polymerized (F-actin) actin to become potent NCs. Here we use the ExoY effector domain (Vn-ExoY) of the *Vibrio nigripulchritudo* Multifunctional-Autoprocessing Repeats-in-ToXin (MARTX) toxin to study ExoY-like toxins that selectively interact with G-actin. Vn-ExoY interacts with only modest affinity with G-actin but can be potently activated by the G-actin:profilin complex, which is abundant in eukaryotic cells. This interaction inhibits the assembly of actin:profilin onto actin filament barbed-ends *in vitro*, whether spontaneous or mediated by formin or VASP elongating factors. High resolution crystal structures of nucleotide-free, 3'-deoxy-ATP- or 3'-deoxy-CTP-bound Vn-ExoY activated by free or profilin-bound G-actin-ATP/-ADP show that the cofactor only partially stabilises the nucleotide-binding pocket (NBP) of NC toxins. Substrate binding promotes a large closure of their NBP. This constrains catalytically important residues around the substrate and promotes the recruitment of two metal ions to tightly coordinate the triphosphate moiety of purine or pyrimidine nucleotide substrates.

Residues that play an important role in both the purinyl and pyrimidinyl cyclase activity of NC toxins are validated in Vn-ExoY and the distantly-related ExoY from *Pseudomonas aeruginosa*. The data conclusively demonstrate that NC toxins employ a similar two-metal-ion mechanism for catalysing the cyclisation reaction of nucleotides of different sizes.

Significance statement

ExoY-like toxins belong to a family of invasive bacterial nucleotidyl cyclases (NCs) that are activated by binding to eukaryotic cofactors in host cells. They alter host cell signalling by overproducing purine and pyrimidine cyclic nucleotides. The molecular and mechanistic details underlying their activation and catalytic specificities are only partially understood. Here we study ExoYs that selectively interact with actin monomers. We show *in vitro* that such ExoYs likely use the actin:profilin complex as physiological cofactor while disrupting its association to actin filaments. Our structural data reveal unprecedented mechanistic details of how NC toxin active site is consecutively remodeled by cofactor and substrate binding, how they can accommodate different sized nucleotides as substrates, and clarify important features regarding their catalytic reaction.

INTRODUCTION

ExoY-like nucleotidyl cyclase (NC) toxins are virulence factors produced by various Gram-negative β- and γ-Proteobacteria (1). They belong to a family of bacterial NCs sharing a structurally-related catalytic NC domain that is inactive within bacteria. Once injected into eukaryotic cells, they bind to specific eukaryotic proteins to be strongly activated. They then display potent NC activities with broad substrate specificity (2-6) and increase the levels of both cyclic purine (cAMP, cGMP) and pyrimidine (cCMP, cUMP) nucleotides, thereby disrupting host cell signalling (reviewed in (1, 2, 7-9)). The Edema Factor (EF) from *Bacillus anthracis* and CyaA toxin from *Bordetella pertussis* both are activated by calmodulin (CaM), whereas the ExoY-like NC toxins use an original cofactor, namely actin (5). While the CaM-activated toxins have been extensively studied over the past decades, the functional specificities and virulence mechanisms of ExoY-like NC toxins remain to be further elucidated.

Exoenzyme Y (ExoY) was first identified in *Pseudomonas aeruginosa* (Pa) as a type III secretion system (T3SS) effector (Pa-ExoY) (10). It was subsequently found to be the second most prevalent T3SS exotoxins encoded in the genomes of clinical or environmental isolates of *P. aeruginosa* (11). Pa-ExoY NC activity in host cells alters the host immune response (12, 13) and leads to the release of cytotoxic amyloids from the pulmonary endothelium, which impairs cellular repair following

infection (8, 14, 15). ExoY-like NC homologues from different pathogens vary considerably in their protein sequence and differ in the actin form they use for activation and in their substrate specificity (1, 6). They are therefore expected to induce a wide variety of cytotoxic effects in infected cells. The MARTX Vn-ExoY module of *Vibrio nigripulchritudo*, an emerging marine pathogen infecting farmed shrimps, shares only 38 % sequence similarity with Pa-ExoY. While Pa-ExoY requires actin filaments (F-actin) for maximum activation (5), Vn-ExoY is selectively activated by G-actin *in vitro* (6). Like EF and CyaA (4), Vn-ExoY shows a strong preference for ATP and can also, with much lower efficiency however, use CTP as substrate (6). Pa-ExoY on the other hand has a broad substrate specificity allowing it to synthesize a variety of cyclic nucleotide monophosphates (cNMPs). The substrate preference we determined *in vitro* is: GTP>ATP≥UTP>CTP (6). In cells, however, ExoY was shown to promote the accumulation of cGMP and cUMP over cAMP and cCMP formation (4). Recently, cUMP and cCMP have been brought to the fore as novel second messengers activating antiviral immunity in bacteria (16) but in eukaryotic cells, the role of these non-canonical second messengers remains largely to be discovered (17).

Bacterial NC toxins belong to the class II adenylate cyclases (ACs). Their catalytic domain may represent a potential drug target against bacterial infections (1, 2) because it is not structurally related to widespread class III mammalian adenylyl or guanylyl cyclases (GCs) that use a dimeric catalytic core (18-23). The monomeric catalytic domain of NC toxins can be divided structurally into subdomains C_A and C_B with the catalytic site located in a groove at their interface (20). EF and CyaA recognise CaM via two flexible regions of C_A that are called switch A (residues 502-551 in EF, 199-274 in CyaA) and switch C (630-659 in EF, 348-364 in CyaA) (20, 21, 24). In CaM-bound EF, switch A and C stabilise another key region of C_A, switch B (578-591 in EF, 299-311 in CyaA), which contains residues that either directly bind ATP or stabilise catalytic residues in the groove between C_A and C_B (20). In EF inactive state, switch B is disordered because switch A and C are stabilised in a conformation oriented away from the catalytic site. Activation of EF or CyaA by CaM does not appear to require a major subdomain movement between C_A and C_B, but does require a CaM-induced movement of switch A and C towards the catalytic site, which in turn stabilises switch B and ATP binding to favour a catalytically competent form of the enzyme (2, 20, 21). This allosteric activation by stabilisation mechanism was recently endorsed for actin-activated NC toxins. In the structure of free Pa-ExoY crystallised by limited in-situ proteolysis, the three switches were not visible in the electron density because they were partially proteolysed and/or flexible (22). Cryo-EM structures of actin-activated ExoY from *P. aeruginosa* and *Vibrio vulnificus* (Vv-ExoY) recently showed that Pa-ExoY and Vv-ExoY also recognise selectively F- or G-actin subunits, respectively, with their central switch A and C-terminal switch C (25). Molecular dynamics simulations suggested that Pa-ExoY binding to F-actin

stabilises its otherwise flexible switch A and C, stabilising the whole toxin, including its NBP (25). Despite many advances (1, 20, 21, 24-30), we are far from understanding the detailed activation mechanism of NC toxins and the different steps and specificities of their catalytic mechanism.

Using *in vitro* functional studies in actin self-assembly and structural studies, we show here that Vn-ExoY is designed to target, be potently activated by profilin-bound G-actin and sequester this complex that is important for the dynamics of F-actin barbed-ends in cells. We initiated the structural study of Vn-ExoY interaction and activation by profilin-bound G-actin using an original functional chimera between Vn-ExoY and profilin. We determined several high-resolution structures of Vn-ExoY in complex with free or profilin-bound actin-ATP/ADP, first without and then with non-cyclisable ATP or CTP analogues in its NBP. These structural data reveal how the catalytic site of NC toxins is consecutively remodeled by cofactor and substrate binding and how their NBP after these consecutive structural adjustments may accommodate large purine or small pyrimidine nucleotides (with double or single carbon-nitrogen ring bases, respectively) for catalysis. The data conclusively demonstrate that NC toxins employ a two-metal-ion and similar mechanism for catalysing the cyclisation reaction of purine and pyrimidine nucleotides.

Results

Vn-ExoY binds to actin monomers with only modest affinity and inhibits actin self-assembly

As a model for ExoY toxins that are selectively activated by G-actin (1), we used a functional Vn-ExoY$^{3412\text{-}3873}$ effector domain/module corresponding to residues 3412 to 3873 of *V. n.* MARTX (6). We first examined the effect of Vn-ExoY on actin-ATP/-ADP self-assembly. To avoid the indirect effects due to ATP depletion by Vn-ExoY AC activity, we used an inactive double mutant K3528M/K3535I called hereafter Vn-ExoY^{DM} (corresponding to Pa-ExoY$^{K81M/K88I}$) (6). Actin polymerisation kinetics were monitored using pyrene-labelled actin, which displays an increase in fluorescence intensity when incorporated into filaments. While inactive Pa-Exo^{K81M} accelerates the rate of actin polymerisation (Fig. 1A) (25), Vn-ExoY^{DM} inhibited the polymerisation rate of both G-actin-ATP-Mg and G-actin-ADP-Mg (Fig. 1B,C). Vn-ExoY thus interacts with G-actin-ATP or -ADP in a very different way than Pa-ExoY. To understand Vn-ExoY inhibitory effect, we examined the association of free or Vn-ExoY^{DM}-bound G-actin with the barbed (+) or pointed (-) ends of filaments. Spectrin-actin or gelsolin-actin seeds were used to initiate elongation at the barbed- or pointed-end, respectively. Interaction of Vn-ExoY^{DM} with G-actin-ATP-Mg inhibited actin assembly at both ends (Fig. 1D). The dose-dependent effects on the elongation rates of barbed- and pointed-ends by Vn-ExoY^{DM} were consistent with the formation of a 1:1 molar complex between G-actin and Vn-ExoY^{DM} that sequesters G-actin with an equilibrium dissociation constant (Kd) of 21 μM (Fig. 1D). To confirm

the binding affinity by direct measurement, we performed fluorescence-detected sedimentation velocity experiments using analytical ultracentrifugation (AUC-FDS) with G-actin-ATP labelled with the fluorescent dye Alexa-488 and unlabelled Vn-ExoY fused to Thioredoxin (Trx-Vn-ExoY). This protein fusion, which is more soluble than Vn-ExoY, was preferred for dose-dependence analyses at high concentrations (Fig. 1E). With free labelled G-actin (0.06 µM) bound to Latrunculin-A, an actin-polymerisation inhibitor, the actin sedimentation coefficient distribution gave a peak centred at an $s_{20,w}$ value of 3.3 S (Fig. 1E, left panel) consistent with a globular actin monomer of 42 kDa. Upon incremental addition of Trx-Vn-ExoY, the sedimentation coefficient distribution of labelled actin shifted to higher s-values (from 3.2 up to 4.7 S), demonstrating the interaction of Vn-ExoY with actin. The peak position and shape were concentration-dependent, and the relative proportion of the larger species in the peaks increased with increasing concentrations of Trx-Vn-ExoY. The titration was consistent with the formation of a 1:1 Vn-ExoY:G-actin complex exhibiting a Kd of 11.7 ± 0.9 µM (Fig. 1E, right panel). Vn-ExoY therefore captures G-actin only with modest affinity to form a complex sequestering G-actin.

Vn-ExoY binds and is activated by G-actin bound to profilin

We next investigated whether Vn-ExoY could compete with G-actin-binding proteins (G-ABPs) in host cells despite its moderate affinity for G-actin (31). We examined the *in vitro* AC activity of Vn-ExoY stimulated by G-actin in the presence of three regulatory G-ABPs that display different binding interfaces on G-actin: (i) a chimeric β-thymosin domain of Thymosin-β4 and Ciboulot proteins, which inhibits actin self-assembly by sequestering G-actin (32), (ii) profilin and (iii) a profilin-like WH2 domain of Cordon-Bleu protein (33). The latter two control unidirectional assembly of actin monomers at filament barbed-ends. At saturating concentrations of these three G-ABPs, only profilin did not interfere with G-actin-induced activation of Vn-ExoY AC activity (Fig. 2A). We then performed AUC-FDS experiments, monitoring the sedimentation behaviour of Alexa-488-labelled-G-actin in the presence of Vn-ExoY, profilin or both proteins. Formation of complexes of increasing size was observed by the shifts from an $s_{20,w}$ value of 3.5 S obtained for the peak of free Alexa488-labelled actin to 4.2 S with profilin (15 kDa), 5.0 S with the larger Trx-Vn-ExoY protein (69.1 kDa), and to a higher value of 5.5 S with both proteins (Fig. 2B), validating the formation of a ternary Vn-ExoY:actin:profilin complex in solution. We next examined whether Vn-ExoY interaction with G-actin was modulated by the simultaneous binding of profilin. We measured the binding strength of Trx-Vn-ExoY^{DM} to fluorescently labelled G-actin-ATP alone or bound to profilin using Microscale Thermophoresis (MST). Titrations of the interaction by measuring changes in fluorescence (Fig. 2C) or MST signal (Fig. S1) show that Vn-ExoY binds with similar affinity to free or profilin-bound G-actin.

The assembly of actin:profilin onto F-actin barbed-ends is inhibited by Vn-ExoY

To understand the impact of Vn-ExoY interaction with actin:profilin on actin self-assembly, we first examined its effects on the spontaneous assembly of actin:profilin at F-actin barbed-ends. We measured the normalised initial rate of barbed-end filament growth in the presence of increasing concentrations of profilin with or without fixed concentrations of Vn-ExoY. Without Vn-ExoY, barbed-end growth was only modestly inhibited by saturating concentrations of profilin as actin:profilin can associate with and elongate F-actin barbed-ends (Fig. 2D). With Vn-ExoY, the dependence of barbed-end growth on profilin concentration shifted to lower values in a Vn-ExoY dose-dependent manner. This shift was consistent with a decrease of the G-actin pool available for barbed-end elongation due to its sequestration by Vn-ExoY. We next examined the effect of Vn-ExoY on actin:profilin assembly at F-actin barbed-ends regulated by VASP or formin processive barbed-end elongation factors. These latter bind to barbed-ends via an F-actin binding domain (called Formin-Homology domain 2 (FH2) in formins) and favour actin:profilin recruitment at barbed-ends by their neighbouring profilin-binding Proline-Rich Motifs (PRMs, which are repeated in formin FH1 domain). Formins or VASP also counteract the barbed-end capping and growth inhibition by capping proteins (CP). The barbed-end growth of F-actin seeds was therefore monitored in the presence of both G-actin:profilin, CP and either the C-terminal FH1-FH2 domains of mouse Dia1 formin (F or mDia1-FH1-FH2, Figure 2E) or full-length human VASP (V, Figure 2F) to get closer to the physiological regulation of F-actin barbed-ends. When actin (1µM) is saturated by profilin (8 µM), actin nucleation is prevented, and no polymerisation occurs (horizontal dashed gray lines). Under these conditions, the addition of 0.35 nM of spectrin-actin seeds induced rapid elongation of the barbed ends of actin filaments (ascending dotted gray curves). In the presence of 2.1 nM CP, this barbed-end elongation was partially inhibited (black dashed curves) but restored by the addition of 3.2 nM mDia1-FH1-FH2 (Fig. 2E, black curves) or 0.22 µM VASP (Fig. 2F, black curves) because the two elongating factors compete with CP on the barbed ends. Further addition of Vn-ExoY at 0.8 or 1.4 µM to mDia1-FH1-FH2 or VASP in the presence of CP inhibited the barbed-end growth from actin:profilin induced by the two elongating factors (blue curves). These inhibitory effects were independent of Vn-ExoY AC activity for the duration of the kinetic experiments (Fig. S2). The interaction of Vn-ExoY with G-actin:profilin therefore impedes the spontaneous or VASP-/formin-mediated assembly of this complex at the most dynamic ends of actin filaments.

Crystal structures of nucleotide-free and 3'-deoxy-ATP-bound Vn-ExoY in complex with actin-ATP/ADP:profilin or actin-ATP

We next investigated the structural mechanism of Vn-ExoY activation by free or profilin-bound G-actin. To improve the crystallisation strategy (see methods), we designed a chimeric protein containing three fused functional domains: Vn-ExoY extended at the C-terminus (Vn-ExoY$^{3455-3896}$, either wild-type or with K3528M/K3535I), a short profilin-binding, Proline-Rich-Motif (PRM) and profilin (Fig. 3A, VnE/VnE^{DM}-PRM-Prof). The chimera sequestered G-actin with about 100-fold higher affinity than the above characterised Vn-ExoY$^{3412-3873}$ module and exhibited strong actin-dependent AC activity at low G-actin concentrations (Fig. 3B-C). Hence the actin-binding domains in both Vn-ExoY and profilin in this chimera appear to be fully functional. Using this chimera (wild-type or double-mutant), we solved two crystal structures at 1.7 Å resolution: (i) VnE^{DM}-PRM-Prof bound to actin-ADP with the actin polymerisation inhibitor Latrunculin B (LatB), and (ii) VnE-PRM-Prof bound to actin-ADP without LatB (Fig. 3D, Table S1). In these structures, profilin is bound to actin-ADP, the PRM to profilin, Vn-ExoY to actin, while residues 3863-3895 connecting Vn-ExoY C-terminus to the PRM are disordered (Fig. 3D, Table S1). Vn-ExoY contacts actin-ADP via its switch A and C, but only switch C is fully ordered. Vn-ExoY switch A disorder (residues 3682-3727) is close to LatB-binding site in actin but solving the structure without LatB only marginally reduced switch A disorder. In this latter structure, the NBP of Vn-ExoY is further stabilised by a sulphate ion (Fig. 3D, VnE-PRM-Prof-SO_4^{2-}:actin-ADP). From these structural data we designed a minimal functional Vn-ExoY module (residues 3455-3863) by removing the C-terminal disordered residues 3864-3895 (Fig. 3A). This Vn-ExoY$^{3455-3863}$ module exhibits similar catalytic activity as our initial Vn-ExoY$^{3412-3873}$ construct. Using this minimal functional domain devoid of its large disordered C-terminal extension, we solved two additional crystal structures at 1.7 and 2.1 Å resolution, respectively: (i) nucleotide-free Vn-ExoY bound to actin-ATP-LatB and profilin, with a sulphate ion in Vn-ExoY NBP (Fig. 3E, Vn-ExoY-SO_4^{2-}:actin-ATP-LatB:profilin), and (ii) Vn-ExoY bound to actin-ATP-LatB with its NBP filled by a non-cyclisable ATP analogue 3'-deoxy-ATP (3'dATP, Figure 3F). The Vn-ExoY-SO_4^{2-}:actin-ATP-LatB:profilin structure is very similar to the structures of the VnE/VnE^{DM}-PRM-Prof chimera bound to actin-ADP, with Vn-ExoY switch A similarly disordered. In contrast, the Vn-ExoY-3'dATP-2Mg^{2+}:actin-ATP-LatB structure co-crystallised with 3'dATP reveals a more ordered Vn-ExoY:actin interface and a distinct conformational state of Vn-ExoY NBP that is more competent for catalysis as described below.

In the G-/F-actin-bound state of ExoYs, their C-switch provides steady interactions while other regions remain dynamic

Vn-ExoY undergoes significant structural rearrangements at both C_A and C_B subdomains between its nucleotide-free conformations bound to actin-ATP/ADP and profilin, and its 3'dATP-bound conformation in complex with actin-ATP (Fig. 4A). At the Vn-ExoY:actin interface, none of the buried

contacts of Vn-ExoY switch C move, except for Leu3827, which is relocated by switch A remodelling (Fig. 4A-B). The switch C thus appears to be essential to initiate the interaction and stabilise Vn-ExoY on actin. In the absence of 3'dATP, most of switch A is too flexible to be modelled and the switch A portions that are ordered in the absence of ligand undergo profound rearrangements following 3'dATP-binding (up to 10 Å on D3682 and K3683 Cα atoms, Figure 4A). Thereafter, the superscript letters after the residue numbering are used to distinguish residues of different proteins and the functional regions/subdomains to which they belong in these proteins (e.g., $^{\text{VnE-CA}}$ refers to residues belonging to Vn-ExoY subdomain C_A). The different conformations of Vn-ExoY bound to actin/actin:profilin with or without a nucleotide substrate analogue allow us to define the mobile "switch" regions as follows: Vn-ExoY switch A as residues Y3675-V3727$^{\text{VnE-Switch-A}}$ (I222-N264$^{\text{PaE-Switch-A}}$, UniProt AC Q9I1S4_PSEAE), switch B as H3753-A3770$^{\text{VnE-Switch-B}}$ (H291-A308$^{\text{PaE-Switch-B}}$), switch C as I3819-L3863$^{\text{VnE-Switch-C}}$ (K347-V378$^{\text{PaE-Switch-C}}$). Other important conformational changes near the interface are in the parts of switch C in contact with switch A and B, and of switch B in contact with switch A and C (Fig. 4A-B). These regions display high B-factors in all the complexes with nucleotide-free Vn-ExoY (Fig. 4D-1). Near the interface, the C_B subdomain of Vn-ExoY undergoes the most drastic global rearrangement with a large 25° rotation as a rigid body around the hinge regions 3532-3533^{VnE} and 3662-3663^{VnE}, thus acting as a lid (called hereafter C_B/LID, residues Lys3533-Met3662$^{\text{VnE-LID}}$, corresponding to Lys86-Met209$^{\text{PaE-LID}}$ in Pa-ExoY) that closes on C_A to stabilise 3'dATP binding (Fig. 4A-B, movie S1A-B). The conformational changes induced by 3'dATP binding bring several regions of Vn-ExoY C_A subdomain closer to actin, increasing the buried solvent-accessible area (BSA) of switch A from 338 to 707 Å^2, reaching the BSA value of switch C (810 and 766 Å^2 respectively). Vn-ExoY interacts with a large surface area of actin, with its switch-A interacting primarily with actin subdomains 2 and 4, and the switch-C with actin subdomains 1 and 3 (Fig. 4C).

To validate the importance of switch C for ExoY proper positioning on actin, we mutated conserved buried residues of switch C that remain well anchored and steady in the complexes with or without 3'dATP. Actin Asp25 (Asp25^{Actin}) forms a buried salt bridge at the interface core with Arg3824$^{\text{VnE-switch-C}}$ side chain (distances of 2.7 and 3.2 Å between N-O atom pairs, Figure 3D-F, 4B-C) and was previously identified as a crucial residue for Pa- and Vn-ExoY activation by F- and G-actin, respectively (5). The Arg3824Ala$^{\text{VnE-switch-C}}$ mutation alone results in a 130-fold reduction in Vn-ExoY G-actin stimulated AC activity (Fig. 5A). Pa-ExoY extreme C-terminus is also crucial for its binding to F-actin (34). The corresponding region in Vn-ExoY is located at the rim of the Vn-ExoY:actin interface, where Vn-ExoY extreme C-terminal amphipathic helix (residues 3847-3863$^{\text{VnE-switch-C}}$) binds into the hydrophobic cleft located between actin subdomains 1 and 3. Mutating the most buried hydrophobic residues of this

amphipathic helix into alanine causes a 240-fold reduction in its AC activity (Fig. 5A). Quite similar interactions exist in the switch C of Pa-ExoY bound to F-actin (25). Three basic amino-acids of Pa-ExoY in proximity of Asp25^{Actin} may play the same role as Arg3824$^{VnE\text{-}switch\text{-}C}$: Lys347$^{PaE\text{-}switch\text{-}C}$, His352$^{PaE\text{-}switch\text{-}C}$ and Arg364$^{PaE\text{-}switch\text{-}C}$. While the Arg364Ala mutation in Pa-ExoY switch C had almost no effect on its F-actin-stimulated GC activity, the Lys347Ala and His352Ala mutations caused a ~15- and ~8-fold reduction, respectively (Fig. 5C), suggesting that these two amino-acids act together as Arg3824$^{VnE\text{-}switch\text{-}C}$. On the other hand, changing the three bulky hydrophobic side chains of Pa-ExoY C-terminal amphipathic helix (i.e. Phe367-Leu371-Phe374, Figure 5B) into alanine caused a ~12,000-fold reduction in F-actin stimulated GC activity (Fig. 5C). These residues in the switch C of Vn-ExoY or Pa-ExoY are conserved in most of their counterparts in other β- and γ-Proteobacteria (Fig. 5D). During the transition of ExoYs to an active conformation, their complex with G-/F-actin is thus stably docked to their cofactor at their switch-C, while other regions remain dynamic to regulate additional functional rearrangements.

Importance of switch A for cofactor specificity and of the C_B/LID closure for nucleotide and Mg^{2+} stabilisation

The overall conformation of Vn-ExoY bound to actin and 3'dATP is very close to that of the *V. vulnificus* Vv-ExoY bound to actin:profilin solved by cryo-EM at 3.9 Å resolution (25) except for a difference in the ExoY topology (see Supplementary Materials). In this last structure, the 3'dATP ligand used to prepare the complex could not be modeled in Vv-ExoY. In the two structures, the switch A of Vn-ExoY or Vv-ExoY adopts a similar conformation between actin subdomains 2 and 4. The binding of Vn-/Vv-ExoY switch A to actin hinders primarily longitudinal inter-subunit contacts in F-actin (Fig. S3A), explaining their preference for G-actin (25). The positioning of Vn-ExoY switch A on G-actin is furthermore incompatible with association of this complex or the ternary Vn-ExoY:G-actin:profilin complex to F-actin barbed-ends (Fig. S3A) and accounts for the inhibitions observed in Figure 1D, 2D-F.

Our different structures shed light on two major successive conformational changes at the NC toxin catalytic site. In the structure of the free/inactive Pa-ExoY (22), the A, B, and C switches were not visible as partially degraded and/or flexible. In our nucleotide-free structures of Vn-ExoY bound to G-actin-ATP/-ADP and profilin (Fig. 3D-E), the Vn-ExoY NBP is still only partially stabilised by cofactor binding (Fig. 4D-1), showing that the cofactor binding is not enough to fully stabilise the NBP and catalytic residues of NC toxins as previously inferred (2, 20, 25). 42 to 46 residues out of 53 from switch-A are still disordered. An SO_4^{2-} ion is bound in Vn-ExoY NBP via residues (K3528$^{VnE\text{-}CA}$, K3535$^{VnE\text{-}LID}$, S3536$^{VnE\text{-}LID}$, K3554$^{VnE\text{-}LID}$) that coordinate the γ- and β-phosphates of 3'dATP when this ligand is bound

(Fig. 4D-2). Binding of the ATP substrate and Mg^{2+} ion in the Vn-ExoY NBP requires that the switch B and the supporting part of switch C are rearranged (Fig. 4D-3). To reach its most favourable binding position, the nucleotide must move ~4 Å (distance between the SO_4^{2-} ion and 3'dATP γ-phosphate) through LID closure (Fig. 4D-3). Structural rearrangements in the switch C region that supports switch B are concomitant with stabilisation of the switch A and substrate analogue (Fig. 4D-4,4D-5). At the final stage, switch B and C are well-ordered, while the entire switch A is stabilised on G-actin (Fig. 4D-5). In the Vn-ExoY-3'dATP-2Mg^{2+}:actin-ATP-LatB structure, switch A ultimately contributes to stabilising the nucleotide base via interactions with $Met3726^{VnE\text{-}switch\text{-}A}$.

Catalytic mechanism of ExoY NC toxins activated by G- or F-actin with purine nucleotides

In the catalytic mechanism of NC toxins, the number of ions required for maximum efficiency, the nature of the catalytic base, or the coordination and role of residues during the different steps of the reaction remain controversial (1, 20, 21, 24-30). In the previously resolved structures of cofactor-bound NC toxins, the nucleotide ligands occupy very different positions in the NBP of activated toxins, being coordinated by one or two metal ions that heterogeneously interact with the nucleotide and toxin residues. In F-actin-bound Pa-ExoY structure, the electron density suggested that a single metal ion was associated with the GTP substrate analogue 3'dGTP bound in Pa-ExoY NBP (25) as in several structures obtained with a CaM-activated EF bound to an ATP analogue (20, 21, 26). In the structure of actin-activated Vn-ExoY bound to 3'dATP, the electronic density and coordination geometry suggested that 3'dATP was coordinated by two Mg^{2+} ions. To unambiguously distinguish metal ions from water, we replaced Mg^{2+} by Mn^{2+} ions and collected an anomalous data set at the manganese absorption edge (see Supplementary Materials). The anomalous difference Fourier map clearly demonstrated that two Mn^{2+} ions were bound to 3'dATP at the positions occupied by the Mg^{2+} ions without any significant changes elsewhere (Fig. 6B). Mg^{2+}_A is pentacoordinated in a square pyramidal geometry by two aspartates $Asp3665^{VnE\text{-}CA}$ and $Asp3667^{VnE\text{-}CA}$, and $His3753^{VnE\text{-}switch\text{-}B}$, which are invariant in all NC toxins (Fig. 6A), an α-phosphate oxygen of 3'dATP, and a water molecule. Mg^{2+}_B is octahedrally hexacoordinated by the same two aspartates (Asp3665/$Asp3667^{VnE\text{-}CA}$), an oxygen from each of the three phosphates of 3'dATP and a water molecule.

Figure 6A summarises the main interactions observed with 3'dATP in the Vn-ExoY-3'dATP-2*Mg^{2+}:actin-ATP-LatB structure, which are extrapolated to the natural substrate ATP. The residues of Vn-ExoY coordinating the nucleotide and metal-ions are indicated in coloured boxes in the first inner shell, and equivalent residues in Pa-ExoY, EF, and CyaA sequences are in the next outer shells. 9 out of the 14 residues binding to substrate and Mg^{2+} ions belong to regions of the enzyme that are flexible and significantly rearranged and stabilised upon binding of cofactor, nucleotide substrate and metals

explaining the low basal activity of the free enzyme (6). All side chain contacts are provided by residues that are invariant or similar in Pa-ExoY, EF, and CyaA, and most interactions are conserved in CaM-activated EF bound to 3'dATP-1Yb^{3+} with a closed LID (PDB 1k90) (20) (Fig. S5D).

To assess the relevance of the observed interactions with the ATP analogue, we mutated some of the conserved residues involved in Vn- and Pa-ExoY and analysed the effect on their AC or GC activity, respectively. His351$^{EF\text{-}LID}$ in EF was proposed to play a role in the 3'OH deprotonation by either acting as an acceptor of 3'OH proton (general base) or facilitating the presence of OH^- ions in the vicinity of the ATP 3'OH group (20, 24, 27-29, 35). His351$^{EF\text{-}LID}$ is conserved in CyaA but the corresponding residue in ExoYs is a lysine: Lys3533$^{VnE\text{-}LID}$ or Lys86$^{PaE\text{-}LID}$ (Fig. 6A). In the active site of actin-bound Vn-ExoY with 3'dATP and 2 Mg^{2+} or 2 Mn^{2+}, Lys3533$^{VnE\text{-}LID}$ side chain is too distant to possibly coordinate the ATP 3'OH moiety if the latter were present. Lys3533Q$^{VnE\text{-}LID}$ or Lys86Q$^{PaE\text{-}LID}$ mutations decrease by only 14- and 12-fold their actin-activated AC and GC activity, respectively (Fig. 6C-D), further suggesting that these residues are unlikely to act as a general base. Next, we examined Lys3528$^{VnE\text{-}CA}$ and Lys3535$^{VnE\text{-}LID}$ that are close to the bridge O3α and non-bridge O2α, O1β and O2γ oxygens of 3'dATP (Fig. 6A). Both side chains are at ~3.4 Å from O3α, Lys3528$^{VnE\text{-}CA}$ is closer to O2α and O2γ (2.8-2.9 Å) than Lys3535$^{VnE\text{-}LID}$, and Lys3535$^{VnE\text{-}LID}$ closer to O1β (3.3 Å). The mutations Lys3528Q$^{VnE\text{-}CA}$ or equivalent Lys81Q$^{PaE\text{-}CA}$ in Pa-ExoY essentially abolished the catalytic activity of these toxins (at least ~23,000-fold reduction). The Lys3535Q$^{VnE\text{-}LID}$ or equivalent Lys88Q$^{PaE\text{-}LID}$ resulted in a 250- and 26-fold decrease in G-/F-actin stimulated Vn-ExoY AC or Pa-ExoY GC activity, respectively (Fig. 6C-D). The invariant His3753$^{VnE\text{-}switch\text{-}B}$, which coordinates $Mg^{2+}{}_A$ and stabilises the purine base via a π-π stacking with its imidazole ring, is specific to NC toxins. $Mg^{2+}{}_A$ is expected to be especially important in the NBP of activated mammalian ACs for coordinating and polarising the 3'OH of ATP to facilitate its deprotonation as a first step in the cyclisation reaction (19, 23, 36). The His3753Q$^{VnE\text{-}switch\text{-}B}$ or equivalent His291Q$^{PaE\text{-}switch\text{-}B}$ mutations strongly reduced the toxin catalytic activity (~13,000-fold reduction), suggesting a critical role for the switch B invariant histidine and $Mg^{2+}{}_A$ in the catalysis of NC toxins.

Structural basis for the pyrimidinyl cyclase activity of ExoYs

The activity of NC toxins as pyrimidine nucleotide cyclases was identified some time ago both *in vitro* (6, 37) and in eukaryotic cells (3, 4) but it remains poorly characterised. Among pyrimidine nucleotides, Vn-ExoY, EF or CyaA all primarily use CTP as substrate, while Pa-ExoY prefers UTP but can also use CTP. To investigate how activated NC toxins can also use small pyrimidine nucleotides as substrates, we solved the structure of Vn-ExoY bound to 3'dCTP in complex with actin-ADP at 2.2 Å resolution (Vn-ExoY-3'dCTP-2*Mn^{2+}:actin-ADP-LatB). This is the first structure of an activated NC

enzyme bound to a pyrimidine nucleotide substrate analogue to be determined. The overall conformation of Vn-ExoY in this structure is identical to those found in the complexes with actin-ATP, 3'dATP and two Mg^{2+} or Mn^{2+}. As in these complexes, the LID of Vn-ExoY is closed on 3'dCTP and two metal-ions coordinate the phosphate moiety of 3'dCTP. In the NBP of Vn-ExoY, 3'dCTP is stabilised by the same residues and types of interactions as 3'dATP (Fig. 7A). The main differences are in the interactions with the nucleotide ribose and base moieties, which are stabilised by fewer and weaker hydrogen bonds and framed by fewer hydrophobic interactions with 3'dCTP than with 3'dATP. With 3'dATP, the ribose is stabilized by L3530$^{\text{VnE-CA}}$ hydrophobic interactions and hydrogen-bonded by K3533$^{\text{VnE-LID}}$ and Asn3759$^{\text{VnE-switch-B}}$ side-chains (Fig. 6A). In the activated structures of Vn-ExoY and tmAC (19) with a NBP closed on an ATP analogue, Asn3759$^{\text{VnE-switch-B}}$ and Asn1025$^{\text{tmAC-IIC2}}$ similarly hydrogen-bond the O4' oxygen of the nucleotide ribose ring (Fig. 6A, 6F). Just as the mutation of Asn1025$^{\text{tmAC-IIC2}}$ reduces the kcat of tmAC by 30-100(38), the mutation of Asn583$^{\text{EF-switch-B}}$ in EF (corresponding to Asn3759$^{\text{VnE-switch-B}}$) reduces the catalytic activity of EF by at least two orders of magnitude (20). These data thus highlight the importance of hydrogen bonds with the nucleotide ribose to position it correctly during the catalysis of class II and III ACs. With 3'dCTP, the electrostatic interactions with the nucleotide ribose are limited to a single, more labile hydrogen bond between the cytidine ribose ring O4' oxygen and a water molecule that is itself coordinated by Asp3756$^{\text{VnE-switch-B}}$ or Asn3759$^{\text{VnE-switch-B}}$. For its coordination by hydrogen bonds, the cytosine base is stabilised by Met3726$^{\text{VnE-switch-A}}$ and Ala3755$^{\text{VnE-switch-B}}$ as the adenine base, but these residues coordinate only the cytosine N4 atom. With 3'dATP, these residues stabilise with shorter hydrogen bonds both the N1 and N6 atoms of adenine. Similarly, in the Pa-ExoY:3'dGTP-1*Mg^{2+}:F-actin structure, both the N1, N2, and O6 guanine atoms are hydrogen-bonded to the Ser292$^{\text{PaE-switch-B}}$, His291$^{\text{PaE-switch-B}}$, and Glu258$^{\text{PaE-switch-A}}$ side chains, respectively (Fig. S5C). The pyrimidine base is otherwise sandwiched by hydrophobic interactions of the Leu3530$^{\text{VnE-CA}}$ and Asn3759$^{\text{VnE-swith-B}}$ side chains and stabilised on the side by hydrophobic interactions of His3753$^{\text{VnE-switch-B}}$ as for the purine base of 3'dATP. The side chain of Pro3760, which further stabilises the imidazole ring of the 3'dATP purine base by hydrophobic interactions on the solvent access side, does not interact with the pyrimidine ring of 3'dCTP. On 3'dCTP triphosphate moiety, the phosphates and two metal ions are tightly coordinated and less solvent-accessible than the nucleoside moiety in Vn-ExoY NBP as with 3'dATP.

To examine whether the conserved interactions with the nucleotide triphosphate moiety play a similar role in the purinyl and pyrimidinyl cyclase activity of ExoYs, we reconsidered the mutations analysed above for Vn-ExoY AC or Pa-ExoY GC activity, now examining their effect on their cytidylyl or uridylyl cyclase (CC/UC) activity (Fig. 7B-C). The mutations with the greatest impact on Vn-ExoY CC or Pa-ExoY UC activity (150- to 480-fold reduction) are those that also most affect their AC or GC

activity, namely K3528Q$^{VnE\text{-}CA}$ or K81Q$^{PaE\text{-}CA}$ and H3753Q$^{VnE\text{-}switch\text{-}B}$ or H291Q$^{PaE\text{-}switch\text{-}B}$, respectively. Like with 3'dATP, K3528Q$^{VnE\text{-}CA}$ side chain hydrogen-bonds α, β, and γ phosphate oxygens of 3'dCTP, and H3753Q$^{VnE\text{-}switch\text{-}B}$ side chain both stabilises Mg^{2+}_{A} via a hydrogen bond and the cytosine base via a π-π stacking with its imidazole ring. In conclusion, these results altogether demonstrate that NC toxins use a similar two-metal-ion catalytic mechanism with purine and pyrimidine nucleotide substrates, which relies on close coordination of their triphosphate moiety for catalysis. The weaker hydrogen bond network around the ribose and base of 3'dCTP likely decreases stability of the pyrimidine nucleoside binding in the NBP of actin-activated Vn-ExoY and may explain why Vn-ExoY remains less efficient as cytidylyl cyclase than adenylyl cyclase (6).

Discussion

Here we used the MARTX Vn-ExoY module to study the functional specificities of ExoY-like toxins that selectively interact with G-actin (6). Our data show that the modest affinity of Vn-ExoY for free G-actin (Fig. 1D-E, Kd~12 µM versus a Kd of ~0.2-20 nM for CyaA or EF binding to CaM(39)) is compensated by its ability to interact and be efficiently activated by G-actin bound to profilin (Fig. 2A-C). In contrast, Vn-ExoY cannot bind to G-actin complexed with other common G-actin binding proteins such as Thymosin-β4, WH2 domains (Fig. 2A) or actin-depolymerising factor (ADF)/cofilin because their binding interfaces between actin subdomains 1 and 3 overlap (Fig. S6). The G-actin:profilin complex is abundant and important to support filament assembly at barbed-ends in eukaryotic cells (31, 40). It is thus likely to represent the major physiological form of G-actin that is recognised and used as a cofactor in eukaryotic cells by Vn-ExoY and closely-related ExoYs. Many ExoY-like homologues from various γ-proteobacteria might indeed be structurally-related to Vn-ExoY (Fig. 5D). The interaction of Vn-ExoY with G-actin:profilin inhibits *in vitro* the spontaneous as well as the formin- or VASP-mediated association of G-actin:profilin complexes with F-actin barbed-ends, independent of the NC activity of the toxin (Figs. 2D-F, S2). It does not, however, prevent profilin from interacting with PRM segments, as shown by the multipartite interactions of our chimera in its complex with actin (Fig. 3D). Further investigations are needed to see whether the formation of such a Vn-ExoY:G-actin:profilin abortive ternary complex for barbed-end elongation, which can be recruited by PRMs of elongation factors or other modular ABPs, may also contribute to Vn-ExoY cytotoxicity in host cells independently of its NC activity. Several observations suggest that Pa-ExoY may also affect eukaryotic target cells independently of its enzymatic activity (5, 41, 42). The interaction of Vn-ExoY with actin:profilin may be especially important for its subcellular localisation and activation at regions of active actin cytoskeleton remodelling, where G-actin:profilin and elongation-promoting factors such as formin or VASP together play important roles (40, 43-45). Localised cAMP synthesis by Vn-

ExoY:actin:profilin may modulate actin cytoskeleton dynamics in various important cellular processes such as cell adhesion and migration (1, 46, 47). At the leading edge of migrating cells, the profilin concentration is important to regulate the balance between linear VASP- and branched Arp2/3-driven actin network assembly supporting filopodia and lamellipodia formation, respectively (45). The Arp2/3 nucleation-promoting factor WAVE2 functions there as an A-kinase-anchoring protein that recruits the cAMP-dependent protein kinase (PKA) to membrane protrusions (48). The activity of VASP, which is important in the immune system's function (49), is also regulated by PKA and PKG (50-52). The interaction and activation of Vn-ExoY-related ExoYs by actin:profilin thus outline promising avenues to elucidate virulence mechanisms that are more specifically associated with the use of actin as a cofactor instead of calmodulin with canonical NC toxins.

Our structural data highlight the distinct role of switches A and C during the interaction of ExoYs with G-/F-actin and how the NBP of all NC toxins is remodelled to reach a catalytically active conformation after cofactor binding. Vn-ExoY switch C interactions at the Vn-ExoY:actin interface remain stable with different conformations of the LID/C_B subdomain and switch A (Figs. 3D-F, 4A-B) and thus firmly docks the toxin to actin. The switch A is only barely stabilised by actin in the absence of substrate (Figs. 3D-E, 4D). After substrate binding, the substrate-stabilised conformation of switch A is significantly different between G- or F-actin specific ExoY NCs (25) (Fig. S8B, S9), which determines their specificity for G- versus F-actin (6, 25). Switch A is furthermore critical to prevent actin:profilin assembly onto F-actin barbed-ends in ExoY:actin:profilin ternary complexes (Figs. 2D-F, S3A). Finally, switch A is the region with the most divergent folding at the toxin:cofactor interface between G-/F-actin-bound ExoYs on the one hand and CaM-bound EF or CyaA on the other hand (Figs. S3B-C, S4), suggesting that this region is essential for establishing the specificity toward different cofactors in NC toxins. The different orientations of the switch A of Vn-ExoY and Pa-ExoY bound to G-actin with 3'dATP or F-actin with 3'dGTP (25), respectively, also induce different orientations of the nucleotide purine base in their NBP (Fig. S9). Further work is needed to understand how this may contribute to their different substrate specificity (6).

In contrast to Vn-ExoY, CyaA or EF have the switch A already fully folded onto CaM in their nucleotide-free cofactor-bound state. Their C_B/LID subdomain can however also adopt different positions in isolated CyaA (53) or between different crystal structures of CaM-bound EF (Fig. 6E, S10). Many crystal structures of CaM-bound EF or CyaA with ligands in their active site were first crystallised without substrate analogues or reaction products and then incubated with these ligands. Crystal packing in these structures may have prevented complete rearrangements of the NBP and LID/C_B subdomain closure. As a result, and due to the intrinsic flexibility of the LID/C_B subdomain, both substrate analogues and metal ions occupy quite different positions in the NBP of CaM-bound EF or CyaA (Figs.

S5, S10) (1). These structures may correspond to intermediate stages of LID/C_B movement and substrate entry. Cofactor binding thus initiates in NC toxins an allosteric stabilisation of switch B by rearranging the central switch A and C-terminal switch C towards switch B as previously reported (2, 20, 25). In the ExoY NC toxins, complete stabilisation of switch A on actin additionally requires substrate binding and C_B/LID closure. Switch A is indeed involved in the correct positioning of the substrate by directly coordinating the purine or pyrimidine base of nucleotides in all cofactor-bound NC toxins (Figs. 6A, 7A, S5, S9). In the inactive conformation of free Pa-ExoY (22) or the nucleotide-free conformations of actin:profilin-bound Vn-ExoY (Fig. 3D-E), His291$^{\text{PaE-switch-B}}$ or His3753$^{\text{VnE-switch-B}}$, respectively, are stabilised away from the NBP by a salt bridge with Asp3736^{VnE}/Asp274^{PaE}, which are located near the switch A (Fig. 4D). After binding to actin, the substrate binding induces in ExoYs the flipping of His3753$^{\text{VnE-switch-B}}$/His291$^{\text{PaE-switch-B}}$ towards the NBP. This invariant histidine of NC toxin switch B aids in the proper positioning of the catalytic Mg^{2+}_{A} onto the two invariant aspartates (Asp3665Asp3667$^{\text{VnE-CA}}$ or Asp212Asp214$^{\text{PaE-CA}}$) with purine or pyrimidine nucleotide substrate analogues (Fig. 6A-B, 7A). In all NC toxins, substrate binding therefore ultimately facilitates the C_B/LID closure. This further stabilises the nucleotide substrate and metal ion binding with more interactions and decreases their degree of freedom in the NBP (Fig. S5) to promote catalysis.

Our data demonstrate unambiguously that Vn-ExoY employs a two-metal-ion-aided catalytic mechanism with purine and pyrimidine nucleotides. Given the sequence similarity and structure conservation, this is very likely to be the case for all bacterial NC toxins after LID/C_B closure (Figs. 6A-B, 7A, S5). Interestingly, the coordination of metal ions and residues of the Vn-ExoY NBP with the ATP-analogue is also more similar to that observed in the structures of activated class III ACs (19) than the coordinations previously observed in the NBP of cofactor-activated NC toxins (Figs. 6A, 6F, S5). The active site of transmembrane or soluble ACs (tmAC/sAC) is built at the interface of their two homologous catalytic domains (called C1 and C2 in tmAC, Figure 6F). It has also been proposed to undergo an open-closed transition during catalysis. However, in the case of tmAC/sAC, the exact role of the open/closed transition of their dimeric NBP and identification of the dynamic active site processes during substrate binding and turnover remain to be clarified (23). In the closed NBP of all ACs, the correct positioning of the different moieties of ATP is essential for catalysis. This is shown by the strong impact of mutations targeting Asn1025$^{\text{tmAC-IIC2}}$ in tmAC (19, 38) or Asn583$^{\text{EF-switch-B}}$ in EF(20) matching Asn3759$^{\text{VnE-switch-B}}$ in Vn-ExoY. These conserved asparagines similarly hydrogen-bond the ribose ring O4' oxygen of the ATP analogue to stabilise its positioning during catalysis (Fig. 6A, 6F). On the phosphate and 3'OH side, where the most important chemical changes occur, the most probable reaction pathway as well as the key interactions during the different steps were examined by computational studies for tmAC with a closed ATP-binding NBP (36) and for EF with an open or nearly-closed ATP-

binding NBP (using PDB 1XFV/1SK6) (27). The proposed reaction model for tmAC fits better the numerous and close interactions around 3'dATP and metal ions in the closed NBP of activated Vn-ExoY. In the proposed substrate-assisted general base catalytic mechanism for tmAC, several residues appear to be particularly important with metal-ion cofactors for lowering the two highest energy barriers of the reaction. First, Lys1065$^{tmAC\text{-}IIC2}$, Mg^{2+}_{A}, Mg^{2+}_{B} and the two conserved Asp396Asp440$^{tmAC\text{-}VC1}$ anchoring metal ions are critical for jointly facilitating the proton transfer from the ribosyl 3′O to a γ-phosphate oxygen (36). Arg1029$^{tmAC\text{-}IIC2}$ is subsequently critical for the concerted phosphoryl transfer step where Lys1065$^{tmAC\text{-}IIC2}$ is also involved. These interactions belong to C1 and C2 structural elements that are distant in the open NBP of tmAC (19). Thus, the tmAC active site can only fully operate when these key elements of C1 and C2 are optimally combined to catalyse all limiting steps of the cyclisation reaction together. In NC toxins, the NBP closure brings together ATP- and metal-ion-coordinating residues belonging to four different regions that are distant from each other without cofactor and substrate. Three of these ATP- and metal-ion-coordinating regions are flexible, and their motion and stabilisation depend on both cofactor and nucleotide binding for switch A and B, and on substrate binding for switch A and C_B/LID (Fig. 6A, 7A). Our mutational analysis in Vn-ExoY and Pa-ExoY highlights Lys3528$^{VnE\text{-}CA}$/Lys81$^{PaE\text{-}CA}$ and His3753$^{VnE\text{-}switch\text{-}B}$/His291Q$^{PaE\text{-}switch\text{-}B}$ that belong to remote regions without cofactor or substrate. Their mutations into Gln (to conserve polar interactions with ATP or Mg^{2+}) strongly alter the AC/GC and CC/UC activity of Vn-/Pa-ExoY, respectively (Figs. 6C-D, 7B-C). These residues are invariant in EF or CyaA and the same mutations on the equivalent Lys58$^{CyaA\text{-}CA}$ and His298$^{CyaA\text{-}switch\text{-}B}$ in CyaA (54, 55) or His577$^{EF\text{-}switch\text{-}B}$ in EF(20) also largely reduce their CaM-stimulated AC activity. These data suggest that these residues play important roles for catalysing limiting steps of the cyclisation reaction by NC toxins. Our data demonstrate that the two residues are correctly positioned and stabilised with two metal ions only after cofactor and substrate binding and LID/C_B closure (Figs. 6A, 7A, S5). Further investigations are required to determine in detail the path of the NC toxin-catalysed reaction and whether His3753$^{VnE\text{-}switch\text{-}B}$ (or the equivalent histidine in other NC toxins) is critical for initiating 3'OH deprotonation via Mg^{2+}_{A}, and Lys3528$^{VnE\text{-}CA}$ (or equivalent) for the phosphoryl transfer step in a manner analogous to Arg1029$^{tmAC\text{-}IIC2}$ in tmAC. The tight coordination of Vn-ExoY, and most likely other NC toxins, with the triphosphate moiety of purine and pyrimidine nucleotides after closure of their C_B/LID subdomain is important for their ability to catalyse the cyclisation reaction of different sized nucleotides. It will be most interesting to compare these structural insights into the broad NC activity of NC toxins with the functional specificities of newly identified bacterial PycC pyrimidine cyclases, which appear to contain conserved catalytic elements of class III cyclase enzymes (16). The data presented here provide functional elements to further investigate the regulated dynamics and activity of NC enzymes, and how canonical and non-canonical cNMPs may

regulate basic cellular and metabolic processes in different subcellular compartments of eukaryotic cells using cell-invading NC toxins as molecular tools of investigation.

Class II (NC toxins) and III ACs may share some important determinants for their catalysis despite the lack of structural homology in their tertiary and quaternary structure. Upon activation, the collapse of their different ATP/metal-ion coordination regions of their catalytic domains towards the active site brings together and constrains all interactions with the different moieties of ATP and metal ions. This open-closed transition may facilitate the conformational changes of the substrate that are predicted by computational studies during the cyclisation reaction (23, 27, 28, 36). For the catalytic domain of cofactor-activated NC toxins, the substrate-induced fit mechanism is controlled by the C_B/LID subdomain, which is in the direct vicinity of the cofactor binding site. Its intrinsic flexibility and substrate-induced closure ensure both good substrate specificity and efficient enzymatic turnover through repeated closure and opening of the C_B/LID for substrate loading/processing and product release (Fig. S11). Without cofactor binding, substrate-induced NBP closure remains unproductive to catalyse the reaction because the A and B switches, and thus part of the coordination of $Mg^{2+}{}_A$ and the substrate nucleoside moiety (Fig. 6A, 7A), are not properly stabilised. Our study thus highlights key steps during the functional transition of the catalytic site of NC toxins to a catalytically competent state, which may represent potential avenues to specifically inhibit these invasive NCs involved in various bacterial infections (1, 2, 7, 8, 56).

Materials and Methods

The Supporting Information (SI) Appendix includes protein constructs, design of the chimeras used for crystallization and methods for protein expression and purification. Methodologies for pyrene-actin polymerization assays, analytical ultracentrifugation, microscale thermophoresis experiments, NC activity assays, protein crystallization and crystallography are also detailed. Data collection experiments were performed on the PROXIMA-1 and PROXIMA-2 beamlines at synchrotron SOLEIL (Saint-Aubin, France).

Data Availability. X-ray crystallography data have been deposited in Protein Data Bank (8BJH, 8BJI, 8BJJ, 8BR1, 8BO1, 8BR0). To see Table S1 in SI Appendix for further details.

ACKNOWLEDGEMENTS. We thank SOLEIL for providing synchrotron radiation facilities and the staff on PROXIMA-1 and PROXIMA-2 beamlines for technical assistance during data collection. We acknowledge the core facilities of Imagerie-Gif, (http://www.i2bc.paris-saclay.fr), supported by “France-BioImaging” (ANR-10-INBS-04-01). This work was supported by the ANR under ANR-18-

CE44-0004 (to L.R., M.T.N., P.R., U.M.), by CNRS (to L.R., P.R., U.M.) and Institut Pasteur under #PTR 43-16 (to U.M.).

Author contributions: L.R. designed research. M.T.N, M.C., A.A.M., and L.R. performed the molecular biology or biochemical experiments, C.V. the AUC experiments, M.T.N, P.R., S.P., and L.R. the crystallisation and crystallographic experiments, D.R.B. and U.M. the Pa-ExoY mutants and NC activity assays. L.R. and M.T.N. designed the figures and wrote the paper. All authors reviewed and edited the article.

The authors declare no competing interest.

REFERENCES

1. Teixeira-Nunes M*, et al.* (2022) Bacterial Nucleotidyl Cyclases Activated by Calmodulin or Actin in Host Cells: Enzyme Specificities and Cytotoxicity Mechanisms Identified to Date. *Int J Mol Sci* 23(12).
2. Tang WJ & Guo Q (2009) The adenylyl cyclase activity of anthrax edema factor. *Mol Aspects Med* 30(6):423-430.
3. Beste KY*, et al.* (2013) Nucleotidyl cyclase activity of particulate guanylyl cyclase A: comparison with particulate guanylyl cyclases E and F, soluble guanylyl cyclase and bacterial adenylyl cyclases CyaA and edema factor. *PLoS One* 8(7):e70223.
4. Beckert U*, et al.* (2014) ExoY from Pseudomonas aeruginosa is a nucleotidyl cyclase with preference for cGMP and cUMP formation. *Biochem Biophys Res Commun* 450(1):870-874.
5. Belyy A*, et al.* (2016) Actin activates Pseudomonas aeruginosa ExoY nucleotidyl cyclase toxin and ExoY-like effector domains from MARTX toxins. *Nat Commun* 7:13582.
6. Raoux-Barbot D*, et al.* (2018) Differential regulation of actin-activated nucleotidyl cyclase virulence factors by filamentous and globular actin. *PLoS One* 13(11):e0206133.
7. Ahuja N, Kumar P, & Bhatnagar R (2004) The adenylate cyclase toxins. *Crit Rev Microbiol* 30(3):187-196.
8. Morrow KA, Frank DW, Balczon R, & Stevens T (2017) The Pseudomonas aeruginosa Exoenzyme Y: A Promiscuous Nucleotidyl Cyclase Edema Factor and Virulence Determinant. *Handb Exp Pharmacol* 238:67-85.
9. Seifert R (2017) cCMP and cUMP Across the Tree of Life: From cCMP and cUMP Generators to cCMP- and cUMP-Regulated Cell Functions. *Handb Exp Pharmacol* 238:3-23.
10. Yahr TL, Vallis AJ, Hancock MK, Barbieri JT, & Frank DW (1998) ExoY, an adenylate cyclase secreted by the Pseudomonas aeruginosa type III system. *Proc Natl Acad Sci U S A* 95(23):13899-13904.
11. Feltman H*, et al.* (2001) Prevalence of type III secretion genes in clinical and environmental isolates of Pseudomonas aeruginosa. *Microbiology* 147(Pt 10):2659-2669.
12. Jeon J, Kim YJ, Shin H, & Ha UH (2017) T3SS effector ExoY reduces inflammasome-related responses by suppressing bacterial motility and delaying activation of NF-kappaB and caspase-1. *FEBS J* 284(20):3392-3403.
13. He C*, et al.* (2017) Bacterial Nucleotidyl Cyclase Inhibits the Host Innate Immune Response by Suppressing TAK1 Activation. *Infect Immun* 85(9).
14. Voth S*, et al.* (2020) Virulent Pseudomonas aeruginosa infection converts antimicrobial amyloids into cytotoxic prions. *FASEB J* 34(7):9156-9179.
15. Renema P*, et al.* (2020) Exoenzyme Y induces extracellular active caspase-7 accumulation independent from apoptosis: modulation of transmissible cytotoxicity. *Am J Physiol Lung Cell Mol Physiol* 319(2):L380-L390.
16. Tal N*, et al.* (2021) Cyclic CMP and cyclic UMP mediate bacterial immunity against phages. *Cell* 184(23):5728-5739 e5716.
17. Seifert R & Schirmer B (2022) cCMP and cUMP come into the spotlight, finally. *Trends Biochem Sci*.
18. Hurley JH (1998) The adenylyl and guanylyl cyclase superfamily. *Curr Opin Struct Biol* 8(6):770-777.
19. Tesmer JJ*, et al.* (1999) Two-metal-Ion catalysis in adenylyl cyclase. *Science* 285(5428):756-760.
20. Drum CL*, et al.* (2002) Structural basis for the activation of anthrax adenylyl cyclase exotoxin by calmodulin. *Nature* 415(6870):396-402.
21. Guo Q*, et al.* (2005) Structural basis for the interaction of Bordetella pertussis adenylyl cyclase toxin with calmodulin. *EMBO J* 24(18):3190-3201.
22. Khanppnavar B & Datta S (2018) Crystal structure and substrate specificity of ExoY, a unique T3SS mediated secreted nucleotidyl cyclase toxin from Pseudomonas aeruginosa. *Biochim Biophys Acta Gen Subj* 1862(9):2090-2103.
23. Steegborn C (2014) Structure, mechanism, and regulation of soluble adenylyl cyclases - similarities and differences to transmembrane adenylyl cyclases. *Biochim Biophys Acta* 1842(12 Pt B):2535-2547.
24. Shen Y, Zhukovskaya NL, Guo Q, Florian J, & Tang WJ (2005) Calcium-independent calmodulin binding and two-metal-ion catalytic mechanism of anthrax edema factor. *EMBO J* 24(5):929-941.

25. Belyy A, Merino F, Mechold U, & Raunser S (2021) Mechanism of actin-dependent activation of nucleotidyl cyclase toxins from bacterial human pathogens. *Nat Commun* 12(1):6628.
26. Shen Y*, et al.* (2004) Structure of anthrax edema factor-calmodulin-adenosine 5'-(alpha,beta-methylene)-triphosphate complex reveals an alternative mode of ATP binding to the catalytic site. *Biochem Biophys Res Commun* 317(2):309-314.
27. Mones L, Tang WJ, & Florian J (2013) Empirical valence bond simulations of the chemical mechanism of ATP to cAMP conversion by anthrax edema factor. *Biochemistry* 52(15):2672-2682.
28. Jara GE & Martinez L (2016) Anthrax Edema Factor: An Ion-Adaptive Mechanism of Catalysis with Increased Transition-State Conformational Flexibility. *J Phys Chem B* 120(27):6504-6514.
29. Gupta M, Alam S, & Bhatnagar R (2006) Kinetic characterization and ligand binding studies of His351 mutants of Bacillus anthracis adenylate cyclase. *Arch Biochem Biophys* 446(1):28-34.
30. Martinez L, Laine E, Malliavin TE, Nilges M, & Blondel A (2009) ATP conformations and ion binding modes in the active site of anthrax edema factor: a computational analysis. *Proteins* 77(4):971-983.
31. dos Remedios CG*, et al.* (2003) Actin binding proteins: regulation of cytoskeletal microfilaments. *Physiol Rev* 83(2):433-473.
32. Didry D*, et al.* (2012) How a single residue in individual beta-thymosin/WH2 domains controls their functions in actin assembly. *EMBO J* 31(4):1000-1013.
33. Husson C, Renault L, Didry D, Pantaloni D, & Carlier MF (2011) Cordon-Bleu uses WH2 domains as multifunctional dynamizers of actin filament assembly. *Mol Cell* 43(3):464-477.
34. Belyy A*, et al.* (2018) The extreme C terminus of the Pseudomonas aeruginosa effector ExoY is crucial for binding to its eukaryotic activator, F-actin. *J Biol Chem* 293(51):19785-19796.
35. Guo Q, Shen Y, Zhukovskaya NL, Florian J, & Tang WJ (2004) Structural and kinetic analyses of the interaction of anthrax adenylyl cyclase toxin with reaction products cAMP and pyrophosphate. *J Biol Chem* 279(28):29427-29435.
36. Hahn DK, Tusell JR, Sprang SR, & Chu X (2015) Catalytic Mechanism of Mammalian Adenylyl Cyclase: A Computational Investigation. *Biochemistry* 54(40):6252-6262.
37. Gottle M*, et al.* (2010) Cytidylyl and uridylyl cyclase activity of bacillus anthracis edema factor and Bordetella pertussis CyaA. *Biochemistry* 49(26):5494-5503.
38. Yan SZ, Huang ZH, Shaw RS, & Tang WJ (1997) The conserved asparagine and arginine are essential for catalysis of mammalian adenylyl cyclase. *J Biol Chem* 272(19):12342-12349.
39. Shen Y*, et al.* (2002) Physiological calcium concentrations regulate calmodulin binding and catalysis of adenylyl cyclase exotoxins. *EMBO J* 21(24):6721-6732.
40. Pimm ML, Liu X, Tuli F, Lojko A, & Henty-Ridilla JL (2021) Visualizing functional human profilin in cells and in vitro applications. *bioRxiv*:2021.2009.2001.458557.
41. Mancl JM, Suarez C, Liang WG, Kovar DR, & Tang WJ (2020) Pseudomonas aeruginosa exoenzyme Y directly bundles actin filaments. *J Biol Chem* 295(11):3506-3517.
42. Silistre H*, et al.* (2021) Prevalence of ExoY Activity in Pseudomonas aeruginosa Reference Panel Strains and Impact on Cytotoxicity in Epithelial Cells. *Front Microbiol* 12:666097.
43. Suarez C*, et al.* (2015) Profilin regulates F-actin network homeostasis by favoring formin over Arp2/3 complex. *Dev Cell* 32(1):43-53.
44. Rotty JD*, et al.* (2015) Profilin-1 serves as a gatekeeper for actin assembly by Arp2/3-dependent and -independent pathways. *Dev Cell* 32(1):54-67.
45. Skruber K*, et al.* (2020) Arp2/3 and Mena/VASP Require Profilin 1 for Actin Network Assembly at the Leading Edge. *Curr Biol* 30(14):2651-2664 e2655.
46. Howe AK (2004) Regulation of actin-based cell migration by cAMP/PKA. *Biochimica et Biophysica Acta - Molecular Cell Research* 1692:159-174.
47. Simao M*, et al.* (2021) cAMP Bursts Control T Cell Directionality by Actomyosin Cytoskeleton Remodeling. *Front Cell Dev Biol* 9:633099.
48. Yamashita H, Ueda K, & Kioka N (2011) WAVE2 forms a complex with PKA and is involved in PKA enhancement of membrane protrusions. *J Biol Chem* 286(5):3907-3914.
49. Estin ML*, et al.* (2017) Ena/VASP proteins regulate activated T-cell trafficking by promoting diapedesis during transendothelial migration. *Proc Natl Acad Sci U S A* 114(14):E2901-E2910.

50. Aszodi A*, et al.* (1999) The vasodilator-stimulated phosphoprotein (VASP) is involved in cGMP- and cAMP-mediated inhibition of agonist-induced platelet aggregation, but is dispensable for smooth muscle function. *EMBO J* 18(1):37-48.
51. Gertler FB, Niebuhr K, Reinhard M, Wehland J, & Soriano P (1996) Mena, a relative of VASP and Drosophila Enabled, is implicated in the control of microfilament dynamics. *Cell* 87(2):227-239.
52. Halbrugge M, Friedrich C, Eigenthaler M, Schanzenbacher P, & Walter U (1990) Stoichiometric and reversible phosphorylation of a 46-kDa protein in human platelets in response to cGMP- and cAMP-elevating vasodilators. *J Biol Chem* 265(6):3088-3093.
53. Malliavin TE (2017) Molecular Modeling of the Catalytic Domain of CyaA Deepened the Knowledge of Its Functional Dynamics. *Toxins (Basel)* 9(7).
54. Glaser P*, et al.* (1989) Identification of residues essential for catalysis and binding of calmodulin in Bordetella pertussis adenylate cyclase by site-directed mutagenesis. *EMBO J* 8(3):967-972.
55. Glaser P*, et al.* (1991) Functional consequences of single amino acid substitutions in calmodulin-activated adenylate cyclase of Bordetella pertussis. *EMBO J* 10(7):1683-1688.
56. Ziolo KJ*, et al.* (2014) Vibrio vulnificus biotype 3 multifunctional autoprocessing RTX toxin is an adenylate cyclase toxin essential for virulence in mice. *Infect Immun* 82(5):2148-2157.
57. Schrödinger L & DeLano W (2020) PyMOL.
58. Jumper J*, et al.* (2021) Highly accurate protein structure prediction with AlphaFold. *Nature* 596(7873):583-589.
59. Adasme MF*, et al.* (2021) PLIP 2021: expanding the scope of the protein-ligand interaction profiler to DNA and RNA. *Nucleic Acids Res* 49(W1):W530-W534.
60. Jubb HC*, et al.* (2017) Arpeggio: A Web Server for Calculating and Visualising Interatomic Interactions in Protein Structures. *J Mol Biol* 429(3):365-371.
61. Schoning-Stierand K*, et al.* (2020) ProteinsPlus: interactive analysis of protein-ligand binding interfaces. *Nucleic Acids Res* 48(W1):W48-W53.

Figure legends

Fig. 1. Vn-ExoY sequesters actin-ATP/ADP monomers in actin self-assembly and exhibits only modest affinity for G-actin-ATP. (A-C) Polymerisation time course of 4 µM ATP-Mg-G-actin (5 % pyrenyl labelled, (A-B)) or 10 µM ADP-Mg-G-actin (10 % pyrenyl labelled, (C)) in the absence (black) and presence of Pa-ExoY^{K81M} (A) or Vn-ExoY^{DM} (B-C) at the indicated concentrations (µM). **(D)** Initial rates of barbed-end growth from spectrin-actin seeds (dark blue) or pointed-end growth from gelsolin-actin seeds (light blue) were measured with 1.5 µM G-actin (10 % pyrenyl labelled) and increasing concentrations of Vn-ExoY^{DM}. Initial rates were calculated from a linear fit to the first 120 s of each time course and normalised by the initial elongation rate with free G-actin. Vn-ExoY^{DM} inhibits both barbed and pointed-end growth by sequestering G-actin with the indicated Kd (µM) for each dose-dependent inhibition. **(E)** AUC-FDS measurement of Vn-ExoY binding affinity for G-actin. Sedimentation coefficient distribution c(s) (left panel) of Alexa-488 labelled-G-actin-ATP (60 nM), bound to the actin-polymerisation inhibitor Latrunculin A (2.5 µM), was determined in the absence and presence of increasing concentrations of unlabelled Trx-Vn-ExoY (from 0.5 to 50 µM). The resulting sw isotherms from c(s) integration are shown in the right panel. In the isotherm plots, solid circles are the sw data from the dilution series, and the solid line is the best-fit isotherm resulting in an estimated Kd of 11.7 µM for the interaction between Trx-Vn-ExoY and G-actin-ATP-Latrunculin-A.

Fig. 2. Vn-ExoY is activated by profilin-bound G-actin and inhibits the spontaneous or regulated assembly of actin-profilin onto F-actin barbed-ends *in vitro*. (A) cAMP synthesis by G-actin-activated Vn-ExoY in the presence of G-ABPs. Reactions containing 5 ng of Vn-ExoY and Latrunculin-A-bound actin at the indicated concentrations (µM) were started by the addition of 2 mM ATP and incubated for 30 min at 30°C. cAMP synthesis was measured in the absence of G-ABPs (black) or presence of two high concentrations (10, 25 µM) of profilin (green), a sequestering β-thymosin (pink) or profilin-like WH2 (purple) domains, which bind to G-actin with a Kd of 0.1, 0.5 and 0.5 µM, respectively(32, 33). **(B)** Formation of the Vn-ExoY:actin:profilin complex by AUC-FDS. Sedimentation coefficient distribution c(s) of Alexa-488 labelled-G-actin (60 nM) was determined alone (gray line) and in the presence of either unlabelled profilin (8 µM; green line), Trx-Vn-ExoY (24 µM; yellow line) or both proteins (red line). **(C)** Measurement of Trx-Vn-ExoY^{DM} binding to free or profilin-bound actin using changes in fluorescence in MST experiments at low ionic strength. Titration of Alexa-488-labelled, Latrunculin-A-bound ATP-G-actin (0.075 µM), alone (cyan) or bound to 4 (red) and 7.9 (green) µM of profilin, by Trx-Vn-ExoY^{DM} for a 2-fold dilution series from 108 to 0.033 µM of Trx-Vn-ExoY^{DM} in MST optimised buffer (to see methods). The insert shows the fluorescence changes in

the raw data and the table the obtained Kd. Error bars are s.d. (n≥3). **(D)** Vn-ExoY inhibits barbed-end elongation by actin-profilin complex. Initial rates of barbed-end growth from spectrin-actin seeds (0.36 nM) were measured as in figure 1D using 2 μM G-actin (5 % pyrenyl-labelled) and increasing concentrations of profilin in the absence and presence of Vn-ExoY at the indicated concentrations. **(E-F)** Vn-ExoY inhibits formin- (E) or VASP-mediated (F) barbed-end elongation from actin-profilin complex. Barbed-end growth from spectrin-actin seeds (0.13 nM), 1 μM G-actin (5 % pyrenyl-labelled), and 8 μM profilin was measured in the absence or presence of 2.1 nM of capping protein (CP), 3.2 nM of FH1-FH2 domains of mDia1 formin (denoted by F) (E) or 0.22 μM of VASP (V) (F) at the indicated concentrations of Vn-ExoY (VnE).

Fig. 3. Crystal structures of Vn-ExoY in different conformational states bound to actin:profilin or actin, obtained by starting with a chimeric protein containing three fused functional domains including Vn-ExoY. (A) Domain diagrams of: (1) the VnE/VnE^{DM}-PRM-Prof chimera used to initiate the crystallographic study containing Vn-ExoY extended at the C-terminus (ExoY$^{3455-3896}$, numbering from Uniprot accession no. (AC) F0V1C5) fused to a short PRM/Proline-Rich-Motif capable of binding to profilin, and human profilin-1 (Uniprot AC P07737), and (2) an optimised shorter Vn-ExoY$^{3455-3863}$ construct that remains as active as our initial longer construct Vn-ExoY$^{3412-3873}$ (5). **(B)** Synthesis of cAMP by actin-activated Vn-ExoY or VnE-PRM-Prof. VnE-PRM-Prof exhibits strong actin-dependent AC activity, which saturates at much lower G-actin concentrations. Reactions containing 5 ng Vn-ExoY or 2 ng VnE-PRM-Prof and actin at the indicated concentrations were started by the addition of 2 mM ATP and incubated for 10 or 30 min at 30°C. **(C)** VnE^{DM}-PRM-Prof sequestered G-actin-ATP with 100-fold higher affinity than Vn-ExoY^{DM} (residues 3412-3873) in the barbed-end elongation. Initial rates of barbed-end growth from spectrin-actin seeds were measured using 2 μM actin (3 % pyrenyl-labelled) and increasing concentrations of VnE^{DM}-PRM-Prof (in red) or Vn-ExoY^{DM} (in blue). **(D)** Structure of nucleotide-free VnE^{DM}-PRM-Prof chimera bound to actin-ADP-LatB. In Vn-ExoY, the C_A subdomain is coloured yellow, and the four flexible regions switch A, switch B, switch C and LID/C_B subdomain in blue, cyan, purple and orange, respectively, here and in all subsequent figures. Disordered regions are shown as dotted lines, the ATP substrate location in Vn-ExoY NBP by its surface in red and the four actin subdomains by numbers in grey. Conserved interactions corresponding to hot spots are indicated by black labels with the Vn-ExoY and actin side chains shown as green and red sticks, respectively. The sulphate ion bound in VnE-PRM-Prof-SO_4^{2-}:actin-ADP structure is superimposed. **(E)** Structure of nucleotide-free Vn-ExoY in complex with actin-ATP-Latrunculin B (LatB) and profilin (Vn-ExoY-SO_4^{2-}:actin-ATP-LatB:profilin). **(F)** Structure of 3'dATP-bound Vn-ExoY in complex with ATP-actin-LatB (Vn-ExoY-3'dATP-2Mg^{2+}:actin-ATP-LatB).

Fig. 4. Conformational changes and sequence diagram of structural rearrangements in actin-bound nucleotide-free Vn-ExoY upon substrate binding. (A) Porcupine plot illustrating the prominent motions, averaged over the first normal mode, between the nucleotide-free and 3'dATP-bound conformations of actin-bound Vn-ExoY. The red arrow length is proportional to the amplitude of Cα atom motions. **(B)** The conformations of Vn-ExoY in the Vn-ExoY-SO_4^{2-}:actin-ATP-LatB:profilin and Vn-ExoY-3'dATP-2Mg^{2+}:actin-ATP-LatB structures (actin and profilin omitted) superimposed on their C_A subdomain. Residues with significant solvent-accessible areas (BSAs) buried by actin are indicated by yellow (BSA ≤ 35 $Å^2$), green (between 35 and 70 $Å^2$) and pink (≥ 70 $Å^2$) balls on their Cα. **(C)** Vn-ExoY-buried actin residues detailing some contacts between the two proteins. The four numbered actin subdomains are shown in different colours. Vn-ExoY residues are boxed with the same colouring code as in (A,B). **(D)** The LID/C_B, switch A, B and C regions of Vn-ExoY are coloured red, light blue, grey and violet in Vn-ExoY-SO_4^{2-}:actin-ATP-LatB:profilin, and orange, blue, cyan and purple in Vn-ExoY-3'dATP-2Mg^{2+}:actin-ATP-LatB, respectively. D-1) In the nucleotide-free complex, switch B and the beginning of switch C in contact with switch A and B are ordered but display relatively high B-factors in Vn-ExoY. The structures are drawn in a cartoon putty representation (57), where the backbone thickness is proportional to the B-factor value. The black dotted lines represent intramolecular interactions between the residues. D-2) The conformations of switch B and C, and residues (L3530-F3531^{VnE}) close to the LID hinge region V3532-K3533^{VnE} are incompatible with 3'dATP binding or the final stabilised conformation of switch A induced by 3'dATP binding. They must be remodelled to avoid steric clashes (red explosion symbols). D-3) Structural rearrangements of switch B and LID. LID closure is stabilised by electrostatic bonds between Lys3535$^{VnE\text{-}LID}$ or Arg3559$^{VnE\text{-}LID}$ and Asp3766$^{VnE\text{-}switch\text{-}B}$ side chains. The red arrows represent the different region movements. D-4) Structural rearrangements of switch A and C. D-5) In this 3'dATP-bound state, switch B and C have B-factors of the same order as those in the overall structure and the entire switch A stabilises on G-actin. Only the region of switch A (residues 3686-3719) that binds between actin subdomains 2 and 4 retains relatively high B-factors.

Fig. 5. Importance of the switch C at the actin:Vn-ExoY interface. (A) cAMP synthesis catalysed by wild-type or switch C mutated Vn-ExoY (residues Q3455-L3863) activated by G-actin. Reactions containing 2.5 or 5 ng for Vn-ExoY and 5, 50 or 100 ng for Vn-ExoY mutants and 3 µM G-actin-ATP-LatB were started by the addition of 2 mM ATP and incubated for 15 or 30 min at 30°C. Values correspond to averages of reactions containing the indicated concentrations of enzymes. **(B)** The extreme C-terminus amphipathic α-helix of Pa-ExoY (residues 365-376 $^{PaE\text{-}switch\text{-}C}$) is depicted in a helical wheel projection using the HeliQuest analysis (http://heliquest.ipmc.cnrs.fr/). **(C)** cGMP

synthesis catalysed by wild-type or switch C mutated Pa-ExoY activated by F-actin. Reactions containing 5 ng Pa-ExoY^{wt} or Pa-ExoY(R364A, K347A, or H352A) or 1 µg Pa-ExoY(F367A-L371A-F374A) and 3 µM F-actin were started by the addition of 2 mM GTP and incubated for 10 min at 30°C. Error bars in (A,C) correspond to s.d. of at least two experimental replicates. In the cryoEM structure of F-actin-bound Pa-ExoY (25), K347, H352 and R364 side chains are at a distance of 3.1, 4.5 and 4.1 Å from Asp25^{Actin} side chain, respectively. **(D)** Phylogenetic tree showing the relationships among ExoY-like proteins/effector domains produced by various β- and γ-Proteobacteria. ExoYs are classified as Vn-ExoY-like or Pa-ExoY-like homologues based on both their sequence similarity and AlphaFold (58) predicted complex with actin (for more details see Fig. S6). A + sign indicates that the residue or structural element of Vn-ExoY or Pa-ExoY is conserved at the same position in the sequence and predicted structure of the ExoY-like homologue.

Fig. 6. ATP substrate-coordination in activated Vn-ExoY and mammalian transmembrane AC (tmAC) and NBP residues important for the purine nucleotide cyclase activities of ExoY NC toxins. (A) Model of ATP binding in activated-Vn-ExoY based on its interactions with 3'dATP in Vn-ExoY-3'dATP-2*Mg^{2+}:ATP-actin-LatB structure. Thresholds used for the interaction detection are those from PLIP (59), Arpeggio web server (60) and the PoseView tool in the web service platform ProteinsPlus (61). **(B)** The model-phased anomalous difference Fourier map from data collected at 6.55 keV shown as a green mesh contoured at 5.0 σ validates the presence of two Mn^{2+} (grey balls) bound to 3'dATP in Vn-ExoY NBP. **(C)** cAMP synthesis catalysed by wild-type or mutated Vn-ExoY (residues Q3455-L3863) activated by G-actin. Reactions containing 10 ng Vn-ExoY, 100 ng Vn-ExoY(K3533Q) or 1 µg Vn-ExoY(K3528Q, K3535Q, or H3753Q) and 3 µM of LatB-Mg-G-actin were started by the addition of 2 mM ATP and incubated for 10-30 min at 30°C. **(D)** cGMP synthesis catalysed by wild-type or mutated Pa-ExoY activated by F-actin. Reactions containing 10 ng Pa-ExoY^{wt}/Pa-ExoY(K86Q or K88Q) or 8 µg Pa-ExoY(K81Q or H291Q) and 3 µM of Mg-F-actin were started by the addition of 2 mM GTP and incubated for 10-30 min at 30°C. **(E)** The LID/C_B subdomain of EF moves also as a rigid body (16° rotation between PDB 1xfz and 1k90) and adopts different positions relative to EF C_A subdomain between the nucleotide-free (1xfz, 1xfy) (24) and nucleotide-bound (1k90) (20) structures of CaM-bound EF, which are overlaid on their C_A subdomains shown in yellow. F) Model of ATP binding in activated class III tmAC based on the structure of type V AC C1a/type II AC C2 heterodimer bound to the ATP analogue RP-ATPαS (PDB 1CJK) (19). The closed NBPs of activated Vn-ExoY and tmAC share similar interactions with ATP analogues. Their conserved asparagine N3759$^{VnE\text{-}switch\text{-}B}$ or N1025$^{tmAC\text{-}IIC2}$ for example similarly hydrogen bonds the ribose ring O4' oxygen of ATP analogues. In

tmAC, the interaction of N1025$^{tmAC-IIC2}$ with ATP appears to be essential for the correct positioning of the nucleotide ribose during catalysis (19, 38).

Fig. 7. 3'dCTP-coordination in actin-activated Vn-ExoY and NBP residues important for CC and UC activity of Vn-ExoY and Pa-ExoY toxins. (A) Model of CTP binding in activated-Vn-ExoY based on its interactions with 3'dCTP in Vn-ExoY-3'dCTP-2*Mn^{2+}:ADP-actin structure. Thresholds used for interaction detection are the same as in Fig. 6A, F. **(B)** cCMP synthesis catalysed by wild-type or mutated Vn-ExoY activated by G-actin. Reactions containing 100 ng Vn-ExoYwt or 1 µg-100 ng (mean) Vn-ExoY(K3528Q, K3533Q, K3535Q, or H3753Q) and 6 µM of Lat.B-Mg-G-actin were started by the addition of 2 mM CTP and incubated for 60 min at 30° C. **(C)** cCMP and cUMP synthesis catalysed by wild-type or mutated Pa-ExoY activated by F-actin. cCMP synthesis was performed by using 1µg-100 ng (mean) Pa-ExoY^{wt} or Pa-ExoY(K81Q, K86Q, K88Q, or H291Q) and 6 µM of Mg-F-actin and reactions were started by the addition of 2 mM CTP and incubated for 60 min at 30° C. cUMP synthesis was performed by using 100-200 ng (mean) Pa-ExoY^{wt} or 1000-100 ng (mean) Pa-ExoY(K81Q, K86Q, K88Q, or H291Q) and 6 µM of Mg-F-actin and reactions were started by the addition of 2 mM UTP and incubated for 60 min at 30° C. In the absence of G-/F-actin, the basal CC and UC activity of Vn-ExoY and Pa-ExoY are 0.007 and 0.003 pmol/min/ng of the enzyme, respectively.

Figure 1

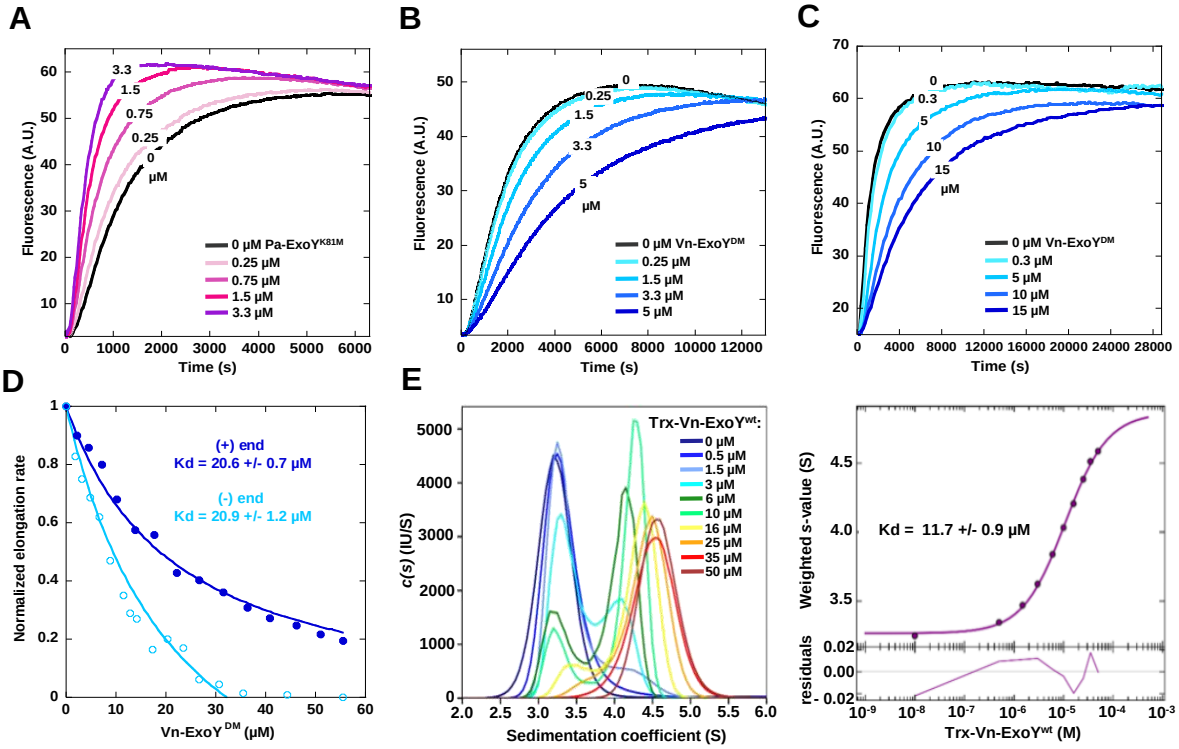
A
Fluorescence (A.U.)
Time (s)
3.3
1.5
0.75
0.25
0
µM
0 µM Pa-ExoY^{K81M}
0.25 µM
0.75 µM
1.5 µM
3.3 µM
B
Fluorescence (A.U.)
Time (s)
0
0.25
1.5
3.3
5
µM
0 µM Vn-ExoY^{DM}
0.25 µM
1.5 µM
3.3 µM
5 µM
C
Fluorescence (A.U.)
Time (s)
0
0.3
5
10
15
µM
0 µM Vn-ExoY^{DM}
0.3 µM
5 µM
10 µM
15 µM
D
Normalized elongation rate
Vn-ExoY^{DM} (µM)
(+) end
Kd = 20.6 +/- 0.7 µM
(-) end
Kd = 20.9 +/- 1.2 µM
E
c(s) (IU/S)
Sedimentation coefficient (S)
Trx-Vn-ExoY^{wt}:
0 µM
0.5 µM
1.5 µM
3 µM
6 µM
10 µM
16 µM
25 µM
35 µM
50 µM
Weighted s-value (S)
Kd = 11.7 +/- 0.9 µM
residuals
Trx-Vn-ExoY^{wt} (M)

Figure 2

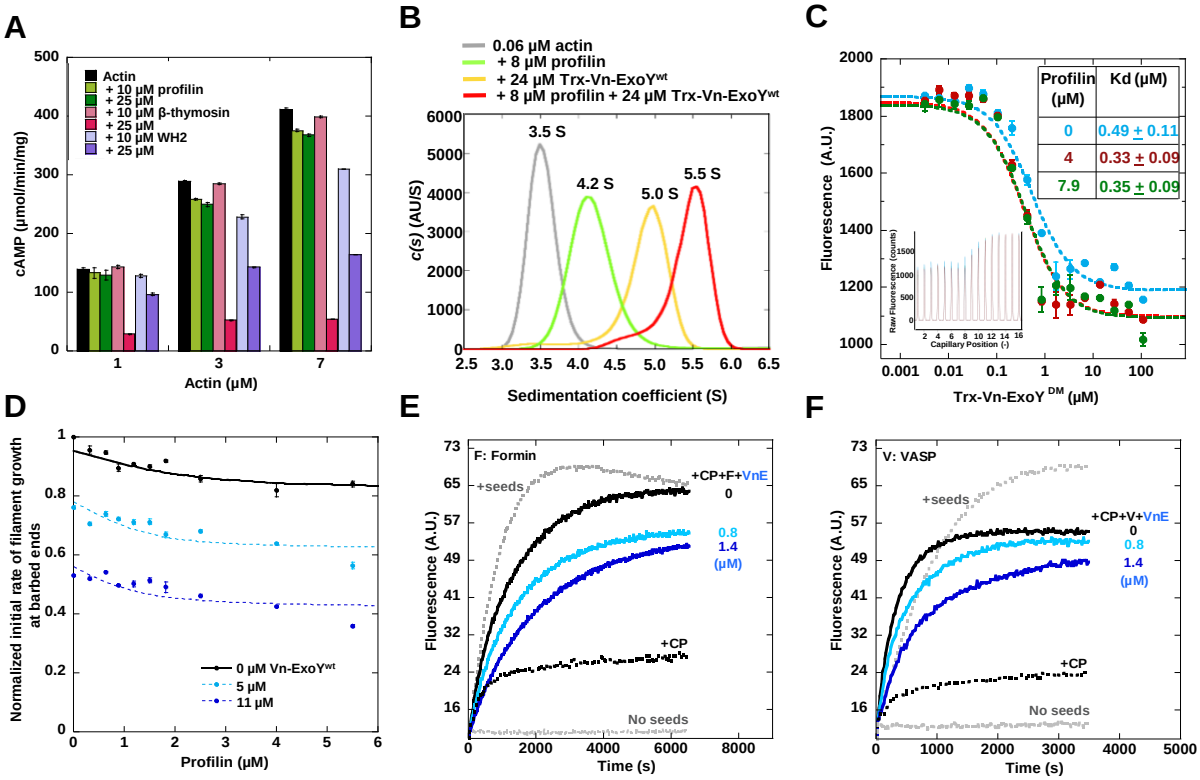
A
Actin
+ 10 µM profilin
+ 25 µM
+ 10 µM β-thymosin
+ 25 µM
+ 10 µM WH2
+ 25 µM
cAMP (µmol/min/mg)
Actin (µM)
B
0.06 µM actin
+ 8 µM profilin
+ 24 µM Trx-Vn-ExoY^wt
+ 8 µM profilin + 24 µM Trx-Vn-ExoY^wt
3.5 S
4.2 S
5.0 S
5.5 S
c(s) (AU/S)
Sedimentation coefficient (S)
C
Profilin (µM)
Kd (µM)
0
0.49 ± 0.11
4
0.33 ± 0.09
7.9
0.35 ± 0.09
Fluorescence (A.U.)
Trx-Vn-ExoY DM (µM)
Raw Fluorescence (counts)
Capillary Position (-)
D
Normalized initial rate of filament growth at barbed ends
0 µM Vn-ExoY^wt
5 µM
11 µM
Profilin (µM)
E
F: Formin
+seeds
+CP+F+VnE
0
0.8
1.4
(µM)
+CP
No seeds
Fluorescence (A.U.)
Time (s)
F
V: VASP
+seeds
+CP+V+VnE
0
0.8
1.4
(µM)
+CP
No seeds
Fluorescence (A.U.)
Time (s)

Figure 3

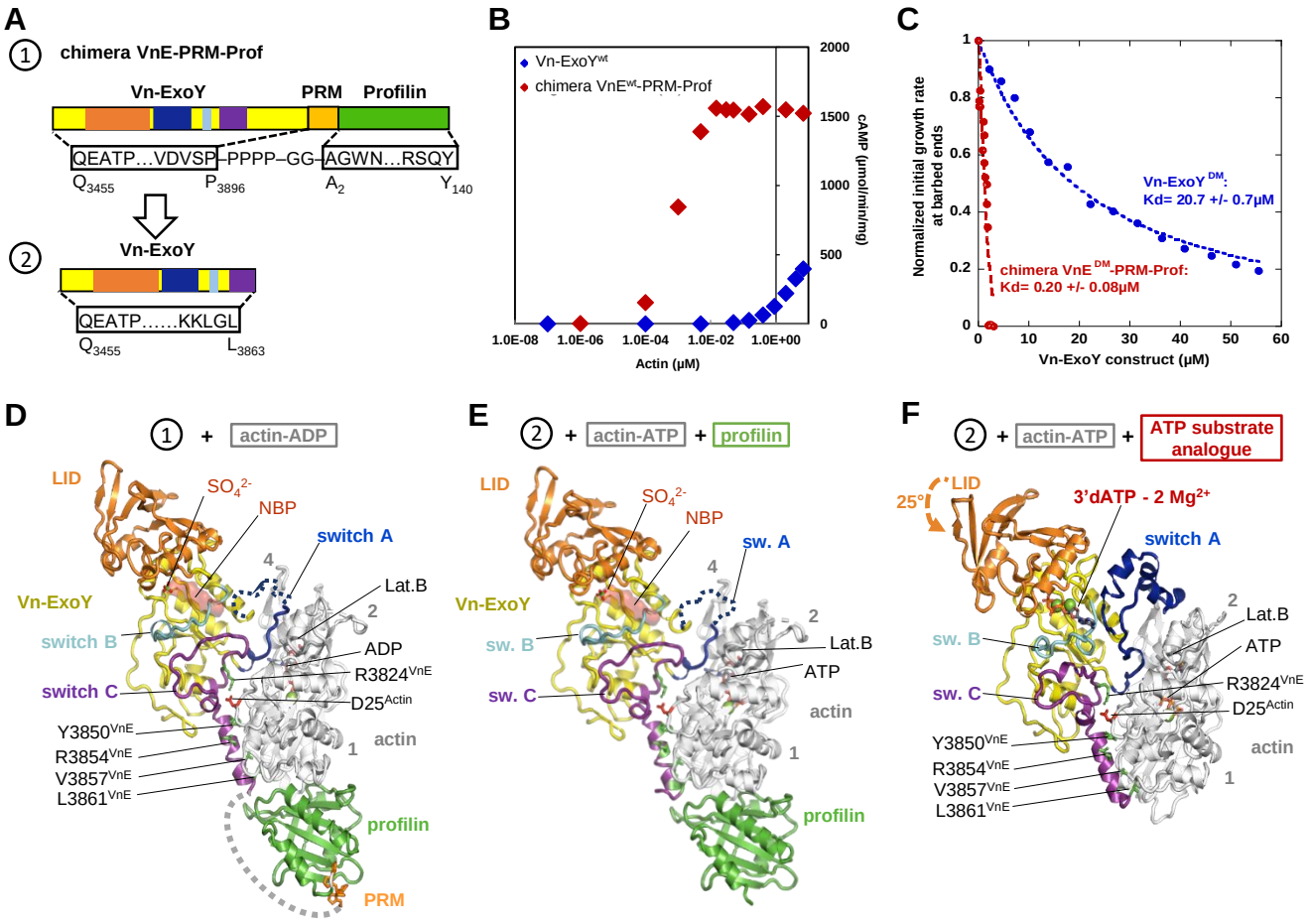
A
1 chimera VnE-PRM-Prof
Vn-ExoY
PRM
Profilin
QEATP…VDVSP–PPPP–GG–AGWN…RSQY
Q3455
P3896
A2
Y140
2
Vn-ExoY
QEATP……KKLGL
Q3455
L3863
B
Vn-ExoYwt
chimera VnEwt-PRM-Prof
cAMP (µmol/min/mg)
Actin (µM)
C
Normalized initial growth rate at barbed ends
Vn-ExoY construct (µM)
Vn-ExoY DM: Kd= 20.7 +/- 0.7µM
chimera VnE DM-PRM-Prof: Kd= 0.20 +/- 0.08µM
D
1 + actin-ADP
LID
SO4 2-
NBP
switch A
Lat.B
Vn-ExoY
switch B
ADP
R3824VnE
switch C
D25Actin
Y3850VnE
R3854VnE
V3857VnE
L3861VnE
actin
profilin
PRM
E
2 + actin-ATP + profilin
LID
SO4 2-
NBP
sw. A
Vn-ExoY
sw. B
Lat.B
ATP
sw. C
actin
profilin
F
2 + actin-ATP + ATP substrate analogue
25°
LID
3'dATP - 2 Mg2+
switch A
Lat.B
sw. B
ATP
R3824VnE
sw. C
D25Actin
Y3850VnE
R3854VnE
V3857VnE
L3861VnE
actin

Figure 4

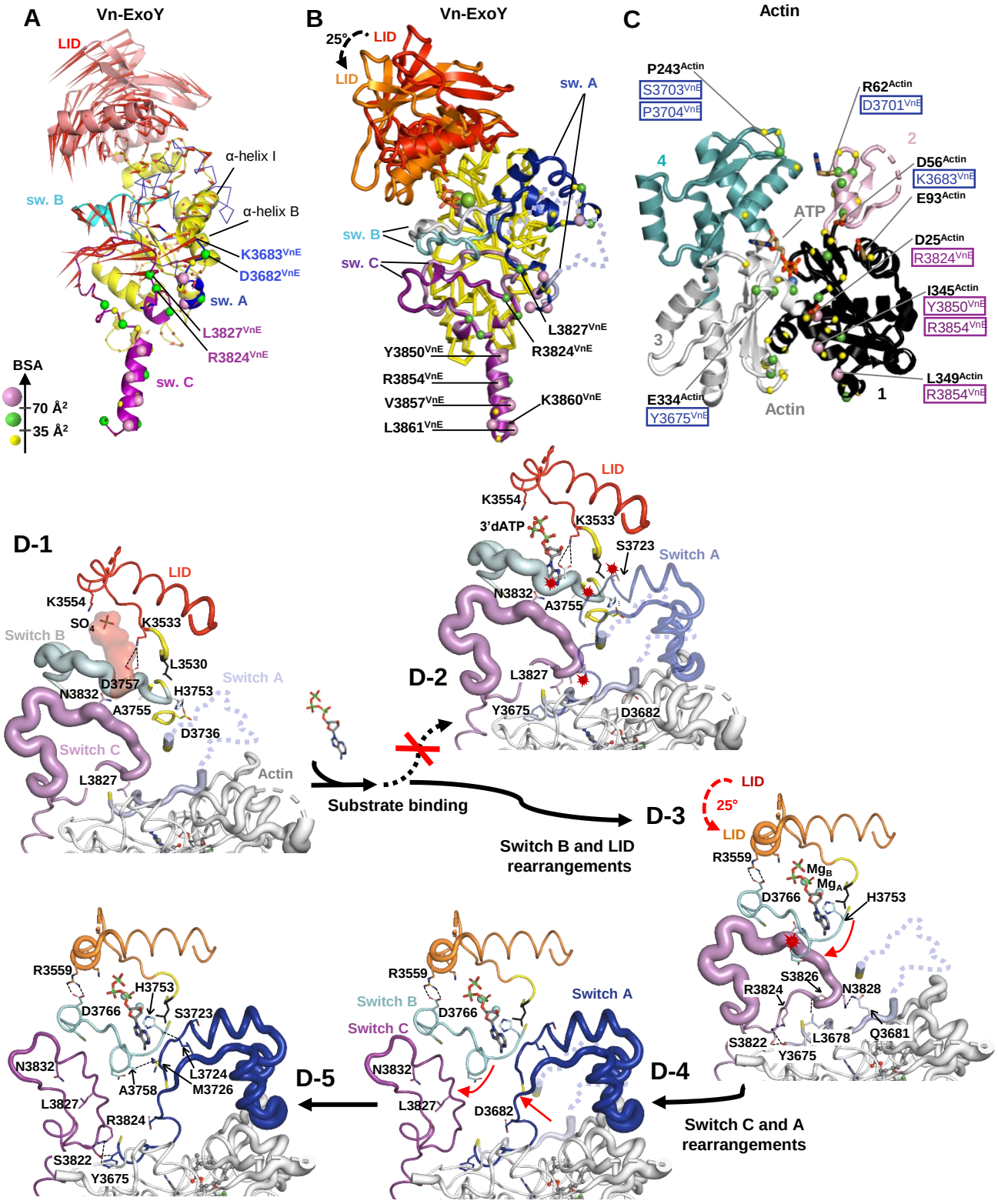
A
Vn-ExoY
LID
α-helix I
sw. B
α-helix B
K3683VnE
D3682VnE
sw. A
L3827VnE
R3824VnE
sw. C
BSA
70 Å²
35 Å²
B
Vn-ExoY
25°
LID
LID
sw. A
sw. B
sw. C
L3827VnE
R3824VnE
Y3850VnE
R3854VnE
V3857VnE
L3861VnE
K3860VnE
C
Actin
P243Actin
S3703VnE
P3704VnE
R62Actin
D3701VnE
2
4
D56Actin
K3683VnE
E93Actin
ATP
D25Actin
R3824VnE
I345Actin
Y3850VnE
R3854VnE
3
L349Actin
R3854VnE
1
E334Actin
Y3675VnE
Actin
D-1
LID
K3554
SO4
K3533
Switch B
L3530
Switch A
D3757
H3753
N3832
A3755
D3736
Switch C
L3827
Actin
Substrate binding
D-2
LID
K3554
3'dATP
K3533
S3723
Switch A
N3832
A3755
L3827
Y3675
D3682
Switch B and LID rearrangements
D-3
LID
25°
LID
R3559
MgB
MgA
D3766
H3753
S3826
R3824
N3828
S3822
L3678
Q3681
Y3675
Switch C and A rearrangements
D-4
R3559
Switch B
Switch A
D3766
Switch C
N3832
L3827
D3682
D-5
R3559
H3753
D3766
S3723
N3832
L3724
A3758
M3726
L3827
R3824
S3822
Y3675

Figure 5

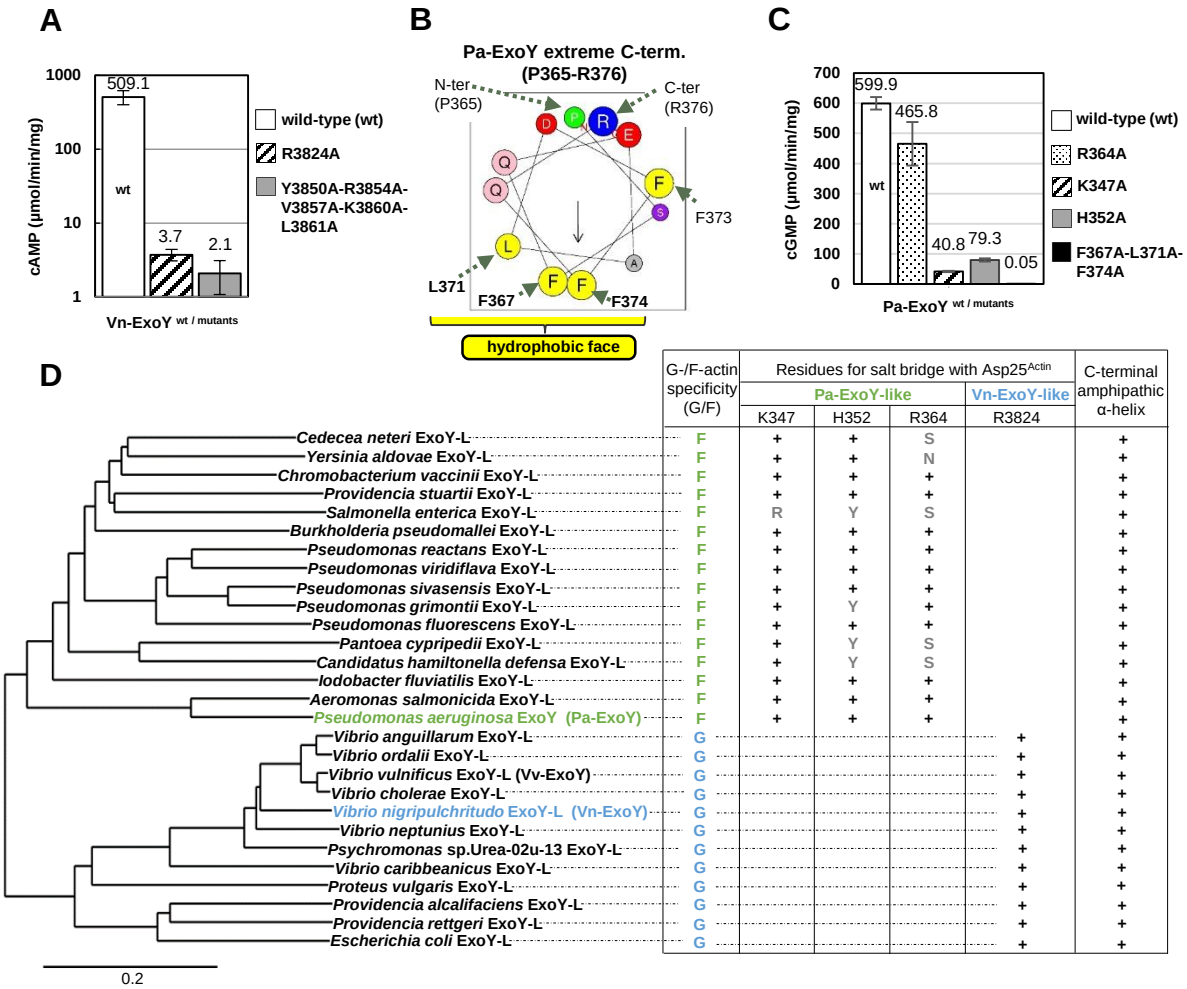
A
1000
100
10
1
cAMP (µmol/min/mg)
509.1
3.7
2.1
wt
wild-type (wt)
R3824A
Y3850A-R3854A-V3857A-K3860A-L3861A
Vn-ExoY wt / mutants
B
Pa-ExoY extreme C-term.
(P365-R376)
N-ter
(P365)
C-ter
(R376)
D
P
R
E
Q
Q
F
S
L
A
F
F
F373
L371
F367
F374
hydrophobic face
C
700
600
500
400
300
200
100
0
cGMP (µmol/min/mg)
599.9
465.8
40.8
79.3
0.05
wt
wild-type (wt)
R364A
K347A
H352A
F367A-L371A-F374A
Pa-ExoY wt / mutants
D
G-/F-actin specificity (G/F)
Residues for salt bridge with Asp25Actin
Pa-ExoY-like
Vn-ExoY-like
K347
H352
R364
R3824
C-terminal amphipathic α-helix
Cedecea neteri ExoY-L F + + S +
Yersinia aldovae ExoY-L F + + N +
Chromobacterium vaccinii ExoY-L F + + + +
Providencia stuartii ExoY-L F + + + +
Salmonella enterica ExoY-L F R Y S +
Burkholderia pseudomallei ExoY-L F + + + +
Pseudomonas reactans ExoY-L F + + + +
Pseudomonas viridiflava ExoY-L F + + + +
Pseudomonas sivasensis ExoY-L F + + + +
Pseudomonas grimontii ExoY-L F + Y + +
Pseudomonas fluorescens ExoY-L F + + + +
Pantoea cypripedii ExoY-L F + Y S +
Candidatus hamiltonella defensa ExoY-L F + Y S +
Iodobacter fluviatilis ExoY-L F + + + +
Aeromonas salmonicida ExoY-L F + + + +
Pseudomonas aeruginosa ExoY (Pa-ExoY) F + + + +
Vibrio anguillarum ExoY-L G + +
Vibrio ordalii ExoY-L G + +
Vibrio vulnificus ExoY-L (Vv-ExoY) G + +
Vibrio cholerae ExoY-L G + +
Vibrio nigripulchritudo ExoY-L (Vn-ExoY) G + +
Vibrio neptunius ExoY-L G + +
Psychromonas sp.Urea-02u-13 ExoY-L G + +
Vibrio caribbeanicus ExoY-L G + +
Proteus vulgaris ExoY-L G + +
Providencia alcalifaciens ExoY-L G + +
Providencia rettgeri ExoY-L G + +
Escherichia coli ExoY-L G + +
0.2

Figure 6

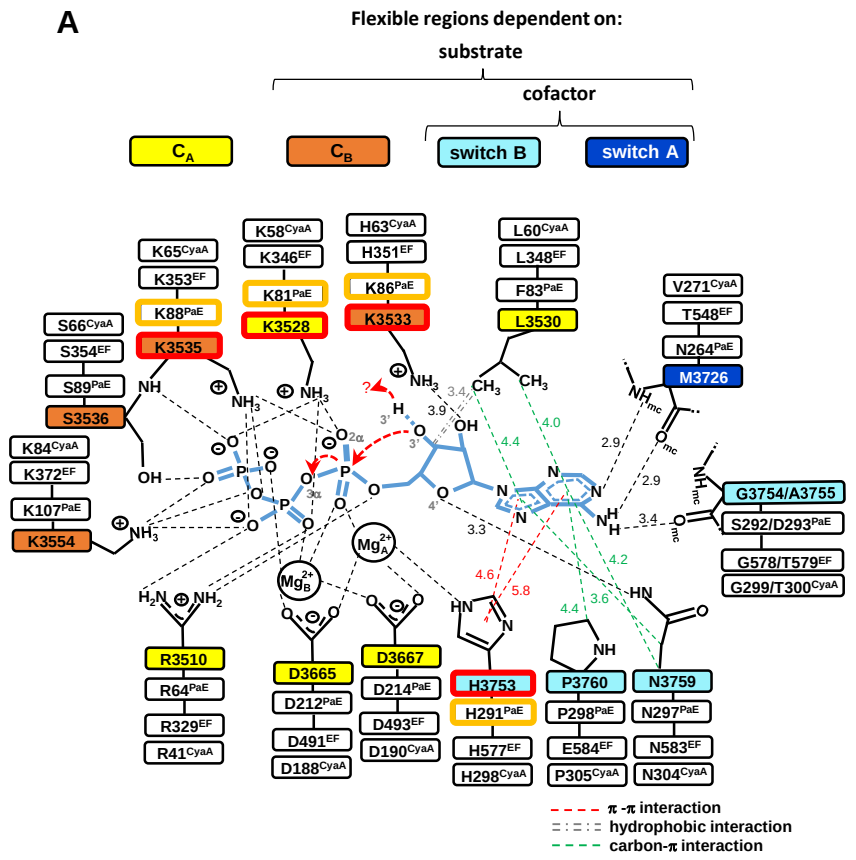
A
Flexible regions dependent on:
substrate
cofactor
C_A
C_B
switch B
switch A
K65CyaA
K353EF
K88PaE
K3535
S66CyaA
S354EF
S89PaE
S3536
K84CyaA
K372EF
K107PaE
K3554
K58CyaA
K346EF
K81PaE
K3528
H63CyaA
H351EF
K86PaE
K3533
L60CyaA
L348EF
F83PaE
L3530
V271CyaA
T548EF
N264PaE
M3726
G3754/A3755
S292/D293PaE
G578/T579EF
G299/T300CyaA
R3510
R64PaE
R329EF
R41CyaA
D3665
D212PaE
D491EF
D188CyaA
D3667
D214PaE
D493EF
D190CyaA
H3753
H291PaE
H577EF
H298CyaA
P3760
P298PaE
E584EF
P305CyaA
N3759
N297PaE
N583EF
N304CyaA
π -π interaction
hydrophobic interaction
carbon-π interaction

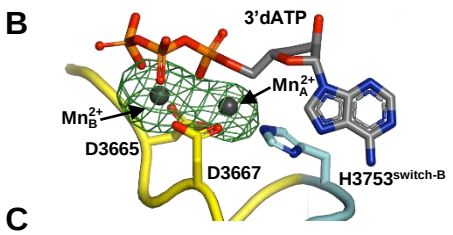
B
3'dATP
Mn_A^{2+}
Mn_B^{2+}
D3665
D3667
H3753switch-B

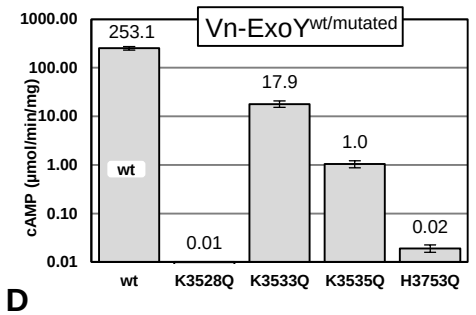
C
Vn-ExoYwt/mutated
cAMP (µmol/min/mg)
1000.00
100.00
10.00
1.00
0.10
0.01
253.1
17.9
1.0
0.01
0.02
wt
wt
K3528Q
K3533Q
K3535Q
H3753Q

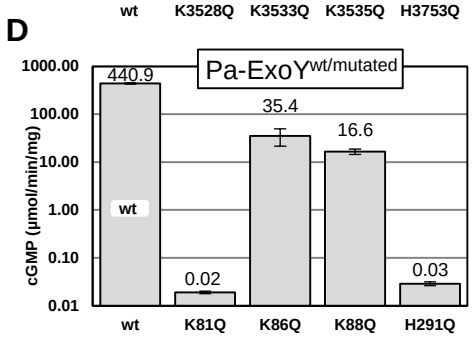
D
Pa-ExoYwt/mutated
cGMP (µmol/min/mg)
1000.00
100.00
10.00
1.00
0.10
0.01
440.9
35.4
16.6
0.02
0.03
wt
wt
K81Q
K86Q
K88Q
H291Q

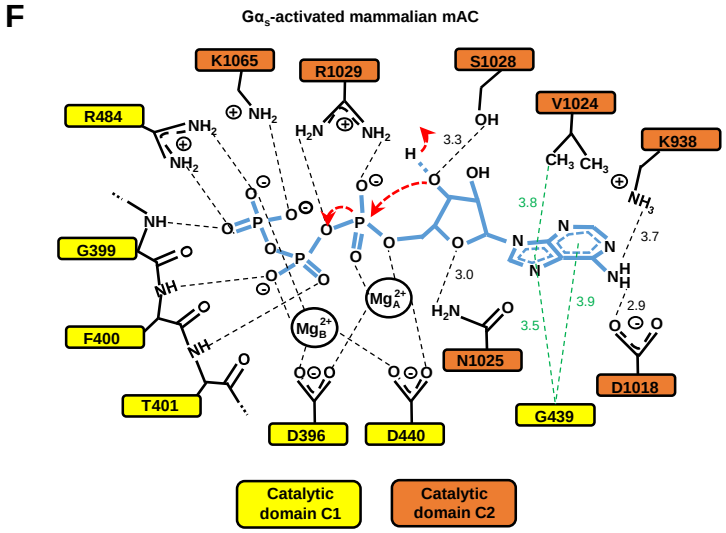
F
Gα$_s$-activated mammalian mAC
K1065
R1029
S1028
R484
V1024
K938
G399
F400
T401
N1025
D1018
D396
D440
G439
Catalytic domain C1
Catalytic domain C2

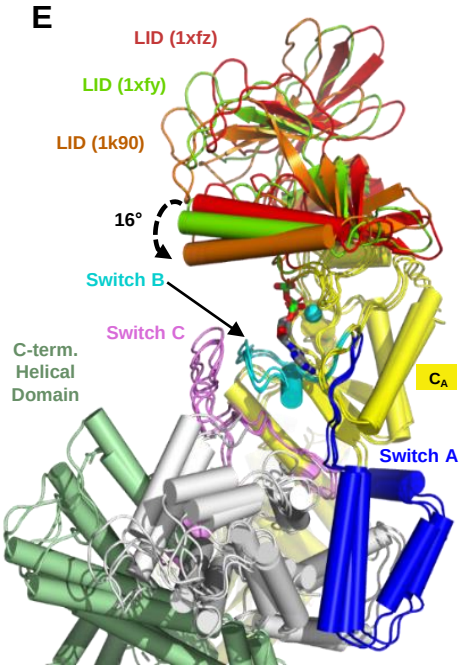
E
LID (1xfz)
LID (1xfy)
LID (1k90)
16°
Switch B
Switch C
C-term. Helical Domain
C_A
Switch A

Figure 7

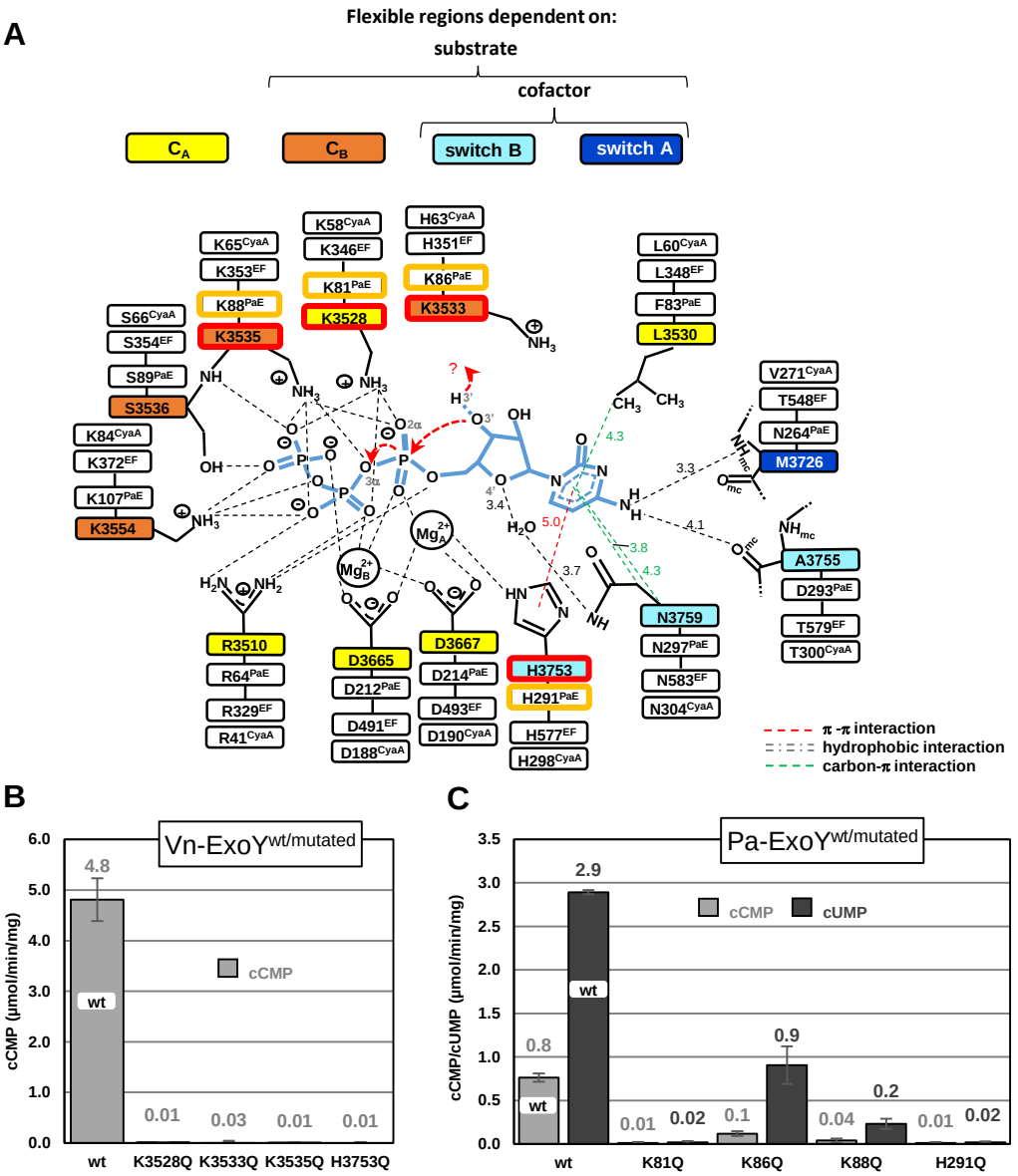
A
Flexible regions dependent on:
substrate
cofactor
C_A
C_B
switch B
switch A
K65CyaA
K353EF
K88PaE
K3535
S66CyaA
S354EF
S89PaE
S3536
K84CyaA
K372EF
K107PaE
K3554
K58CyaA
K346EF
K81PaE
K3528
H63CyaA
H351EF
K86PaE
K3533
L60CyaA
L348EF
F83PaE
L3530
V271CyaA
T548EF
N264PaE
M3726
A3755
D293PaE
T579EF
T300CyaA
R3510
R64PaE
R329EF
R41CyaA
D3665
D212PaE
D491EF
D188CyaA
D3667
D214PaE
D493EF
D190CyaA
H3753
H291PaE
H577EF
H298CyaA
N3759
N297PaE
N583EF
N304CyaA
π -π interaction
hydrophobic interaction
carbon-π interaction
B
Vn-ExoY wt/mutated
cCMP (µmol/min/mg)
cCMP
wt
4.8
0.01
0.03
0.01
0.01
wt
K3528Q
K3533Q
K3535Q
H3753Q
C
Pa-ExoY wt/mutated
cCMP/cUMP (µmol/min/mg)
cCMP
cUMP
2.9
0.8
0.01
0.02
0.1
0.9
0.04
0.2
0.01
0.02
wt
K81Q
K86Q
K88Q
H291Q